HELLENIC REPUBLIC
National and Kapodistrian University of Athens
EST. 1837

Faculty of Geology & Geoenvironment
Department of Geophysics & Geothermy

Application of Ground Penetrating Radar (GPR) technique for archaeological investigations in the region of Plasi, Marathon (Attika)

Igli Muskaj

Supervisor: Ioannis Alexopoulos, Associate Professor of Applied Geophysics

Athens 2023

Contents

Acknowledgments

In this thesis, titled ''Application of Ground Penetrating Radar (GPR) for archaeological investigations in the region of Plasi in Marathon'', are presented the results from the processing and interpretation of the data that were acquired from the geophysical survey that took place in the region of Plasi, Marathon.

The geophysical method used was the reflection of electromagnetic waves utilising a ground penetrating radar. The aim of the research was to identify probable archaeological targets and indicate places of excavation interest.

The assignment and supervision of this thesis was done by Professor Ioannis Alexopoulos to whom I would like to express my gratitude. His expertise with both the subject matter and the process of thesis writing were both invaluable for the completion of this thesis.

I would also like to thank Ioannis Giannopoulos MSc candidate for his help regarding the acquisition, processing and interpretation of the GPR data.

Special thanks to Vasileios Gosios MSc candidate, Georgia Mitsika MSc and Dr. Spiridon Dilalos for the advice they gave me and for the scientific conversations we had.

Finally, I would like to show my appreciation to my friends and family who have supported me over the years throughout my geological journey.

Abstract

The present thesis is focused on the geophysical research that took place in the region of Plasi in Marathon, by the joint efforts of the Department of Geology and Geoenvironment and Department of History and Archaeology, both from the National and Kapodistrian University of Athens. The goal of this research was to locate possible buried archaeological remains and to identify new potential sites of interest in the selected area for further excavation, through a detailed geophysical survey.

The plain of Marathon is an area filled with clastic sediments of Holocene and pre –Holocene age with the investigated area having mainly clayey soil.

The method used for this investigation was the electromagnetic reflection technique, utilizing a Ground Penetrating Radar (GPR). The data acquisition was done with the MALÅ Geoscience monostatic GPR system, equipped with a 250 MHz shielded antenna. A total of 72 2D profiles (radargrams) were acquired in 2 different directions North-South and East-West, in a grid of 50x50cm spacing. Furthermore, the differential Global Positioning System (*dGPS*) and the RTK (*Real Time Kinematics*) technique was used in order to acquire the coordinates for each profile.

The analysis, processing, and interpretation of the GPR data was done using the MALÅ Vision Software, which also provided us with the option to display the GPS data of every 2D profile.

Furthermore, the 72 processed radargrams were interpolated and the final 3D results were presented via 2 methods. Initially, in 2D Depth Slices, which depicted the intensity of the GPR signals that were reflected at a given depth, and secondly, as ISO Surfaces where the intensity of the reflected GPR signals were shown in 3D volumes.

The final results of the geophysical survey highlighted various areas of high reflection intensity and geometrical spatial distribution, in depths between 20cm to 80cm, which seems to relate with the archaeological findings of recent excavations nearby the survey area.

Εφαρμογή της τεχνικής γεωραντάρ (GPR) στην αρχαιολογική έρευνα της περιοχής Πλάσι, Μαραθώνα (Αττική)

Περίληψη

Η παρούσα διπλωματική εργασία επικεντρώνεται στη γεωφυσική έρευνα που πραγματοποιήθηκε στην περιοχή Πλάσι στον Μαραθώνα, από το Τμήμα Γεωλογίας και Γεωπεριβάλλοντος σε συνεργασία με το Τμήμα Ιστορίας και Αρχαιολογίας, του Εθνικού και Καποδιστριακού Πανεπιστημίου Αθηνών. Στόχος της έρευνας ήταν, μέσω μιας λεπτομερούς γεωφυσικής διασκόπησης, να εντοπιστούν πιθανά θαμμένα αρχαιολογικά κατάλοιπα και να αναγνωριστούν νέες θέσεις ενδιαφέροντος για περαιτέρω ανασκαφή.

Από γεωλογικής άποψης, η πεδιάδα του Μαραθώνα έχει πληρωθεί με κλαστικά ιζήματα, ολοκαινικής και προ-ολοκαινικής ηλικίας. Η περιοχή Πλάσι όπου διεξήχθη η γεωφυσική διασκόπηση αποτελείτε κυρίως από αργιλικά ιζήματα, ιδίως στα ανωτέρα τμήματα του εδαφικού ορίζοντα.

Η μέθοδος που χρησιμοποιήθηκε για την διερεύνηση του υπεδάφους, ήταν η τεχνική της ανάκλασης ηλεκτρομαγνητικών κυμάτων με την χρήση γεωραντάρ (GPR). Η λήψη των δεδομένων πραγματοποιήθηκε με ένα μονοστατικό σύστημα γεωραντάρ της MALÅ Geoscience, εξοπλισμένο με μια θωρακισμένη κεραία συχνότητας 250 MHz. Αποκτήθηκαν συνολικά 72 δισδιάστατα προφίλ (*ραδιογράμματα*) σε 2 διαφορετικές κατευθύνσεις Βορρά-Νότος και Ανατολή-Δύση, δημιουργώντας έναν κάναβο με ισοδιάσταση 50cm. Επιπλέον, χρησιμοποιήθηκε διαφορικό GPS και η τεχνική RTK (Real Time Kinematics) για την λήψη των συντεταγμένων για κάθε προφίλ.

Η ανάλυση, επεξεργασία και ερμηνεία των δεδομένων GPR έγινε με τη χρήση του λογισμικού MALÅ Vision, το οποίο παρείχε επίσης τη δυνατότητα να αποτυπωθούν σε χάρτη οι συντεταγμένες για κάθε δισδιάστατο προφίλ.

Τα τελικά αποτελέσματα της γεωφυσικής έρευνας ανέδειξαν διάφορες περιοχές όπου παρατηρούνται υψηλές εντάσεις ηλεκτρομαγνητικής ανάκλασης, οι οποίες παρουσιάζουν μια γεωμετρική χωρική κατανομή. Τα βάθη όπου παρατηρούνται τα αποτελέσματα αυτά κυμαίνονται από 20 cm έως 80 cm, το οποίο φαίνεται να συνάδει με τα αρχαιολογικά ευρήματα των πρόσφατων ανασκαφών που έλαβαν χώρα κοντά στην περιοχή μελέτης.

1.Introduction

The study area belongs to the Municipality of Marathon, of the Eastern Attica Regional. It is the fifth largest municipality in the prefecture of Attica. The University excavation site of the Department of History and Archeology of NKUA is located at the central part of the Marathon plain, next to the coast, 1.5 km northeast of the Tomb of Marathon and 2 km southwest of the Battle Trophy (figs. 1.1, 1.2). It is an area between the two streams of the river Oinois, Haradros to the east and Kainourios to the west.

***Figure 1.1**: Historical map of the broader Marathon area (source: https://digi.ub.xn--uniheidelberg-dm6g.de/diglit/curtius1900a/0007/image).*

Figure 1.2: *Satellite image of the wider area of Marathon (source: google earth).*

From the historical information gathered over the years, we know that Marathon was an important municipality of the city-state of ancient Athens. In the archaic years (700-480 BC), before the Persian wars, it was not of particular historical importance, but it is known that there was a Municipality of Marathon. Plutarch informs us that the Persians, before the battle of Marathon, destroyed and plundered the municipality due to it being very close to their camp. During the classical and Hellenistic years (480-146 BC) because of the Persian wars, for symbolic reasons, the municipality acquired great importance for ancient Athens. It was one of the most important pilgrimages a young Athenian had to make. However, it remains unknown where the seat of the Municipality of Marathon was during the archaic, classical and Hellenistic periods, as the excavations so far, apart from some isolated farmhouses, have not yet revealed an urban fabric with dense population (*info Assoc. Prof. I. Papadatos*).

1.1 Geological - Geomorphological conditions

From a geological perspective, the study area is part of the unit of NW Attica, which belongs to the central Hellenides. According to Lozios (1993), the region represents a metamorphic unit and consists of a metavolcano-sedimentary sequence at the base (Upper Triassic) and an overlying carbonate sequence (U. Triassic – U. Cretaceous), consisting of different phases of marbles and meta-flysch on the roof (Eocene).

The carbonate sequence appears in the wider area, with the following formations:

- **Marbles (MRm)**: Ashy in colour and in places white, crystalline, interstratified to thick-stratified, without shale interlayers, A. Triassic – A. Cretaceous age

- **Marbles (MRp)**: White crystalline or cyanic marbles, which characterize the central part of the area and are in a lateral development at the lower layers of the carbonate sequence.
- **Shales**: They are mainly chloritic, with layers of impure marbles and marbles with silex. They show great variation in their thickness.

The younger post-alpine formations show a significant spread in the area, as the plain has been filled with clastic sediments originated from rivers, lakes, lagoons and seas, of Holocene age. (Lozios,1993; Seni, et al., 2010).

The post-alpine formations that are found in the area are the following:

- **Alluvial deposits (Holocene)**: loose brown clay-sandy materials with scattered cobblestones, chert, floodplain materials and coastal formations.
- **Alluvial deposits (Pleistocene)**: usually brownish-red in colour with scattered cobblestones.
- **Terrestrial deposits (Pleistocene)**: old sedimentary deposits and refined materials.
- **Coarse deposits (Upper Miocene)**: fluvial formations are located on the edges of the mountain masses and consist of marls, clays, sandstones, cobbles, etc. As we move away from the edges they alternate with more detailed materials.

Figure 1.3: *The University archaeological excavation in Plasi, Marathon (photo material by I. Papadatos).*

1.2 Geophysical investigation – Data acquisition

The geophysical survey was carried out in a selected area on the southern part of the University excavation site (fig. 1.4). Preliminary excavations had been done in the area, where archeological remains of various structures dating from the late classical and Hellenistic periods had been revealed. The aim of the geophysical survey was to investigate the existence and spatial distribution of possible remains in the area. Based on the prior information from the excavated sections and the geological

and geomorphological characteristics of the field, it was decided that the geophysical survey should be performed with the use of a Ground Penetrating Radar (GPR).

Figure 1.4: *Satellite image depicting the area where the GPR survey took place (displayed with a rectangle). The starting and the ending points of each GPR profile are presented with green and red colour respectively. (Google earth).*

For the data acquisition, a grid was set on the survey area with one direction being NNW-SSE and the other being NNE-SSW (fig.1.4). By doing so, we had a clear indication of the acquisition paths (Fig. 1.5). In total, 72 2D profiles were acquired using the monostatic GPR system from MALÅ Geoscience with a shielded antenna of 250 MHz frequency (fig. 1.6).

- 31 profiles with 15 m length each and a direction of NNW-SSE with a spacing distance of 0.5 m.
- 41 profiles with 20 m length each and a direction of NNE-SSW with a spacing distance of 0.5 m.

Table 1.1: GPR parameters	
Central frequency of antenna (f_c)	250MHz
Sampling frequency (f_s)	2611MHz
Time sampling rate (Δt_s)	512ns
Spatial sampling rate (Δx_s)	0.02m
Time window (W_t)	192ns
Stacking	16

Figure 1.5: *Picture of the survey area while the grid is being set.*

Figure 1.6: *Picture of the survey area with the grid set and the surveying team ready to start the data acquisition.*

1.3 Topographic corrections

For a geophysical investigation to yield the best results possible, it is always advised to take into consideration the topography of the area and acquire the coordinates of the measurements that are taken, regardless of the geophysical method being used. To achieve this, a local topographic reference **Base** was established at the University excavation site by the research team of the Department of Geology & Geoenvironment (fig 1.7).

In order to accurately determine the coordinates of the **Base** of the topographic reference, the static technique was used with a pair of dual-frequency GPS Hiper receivers with positioning accuracy of 10mm ± 1.0ppm horizontally and 15mm ± 1.0ppm vertically. The dependence and solution were carried out by the network of the company *TREE OMPANY CO A.E.V.E.E.* The reference system used in all topographical surveys is Greek Grid (EGSA'87).

Afterwards, for the topographic mapping (scanning) of all the measurements, the RTK-GPS (Real Time Kinematics) technique was used with Hiper-Pro (Base & Rover) receivers from the company TopCon and the field software TopSurv from the same company (fig. 1.8). The coordinates were calculated with the TopCon Tools software. The horizontal measurement accuracy with this equipment is 0.1 cm and the height measurement accuracy is 1.5 cm.

Figure 1.7: *Topographic reference Base set near the area of interest.*

Figure 1.8: *Acquisition of dGPS data.*

2. Ground Penetrating Radar - GPR

GPR is a geophysical method that can create a high-resolution continuous section that depicts subsurface features in a non-invasive manner. The measurements are mainly done on the ground and the aim is to visualize layers, their presence and continuity in space and to estimate the position of buried objects.

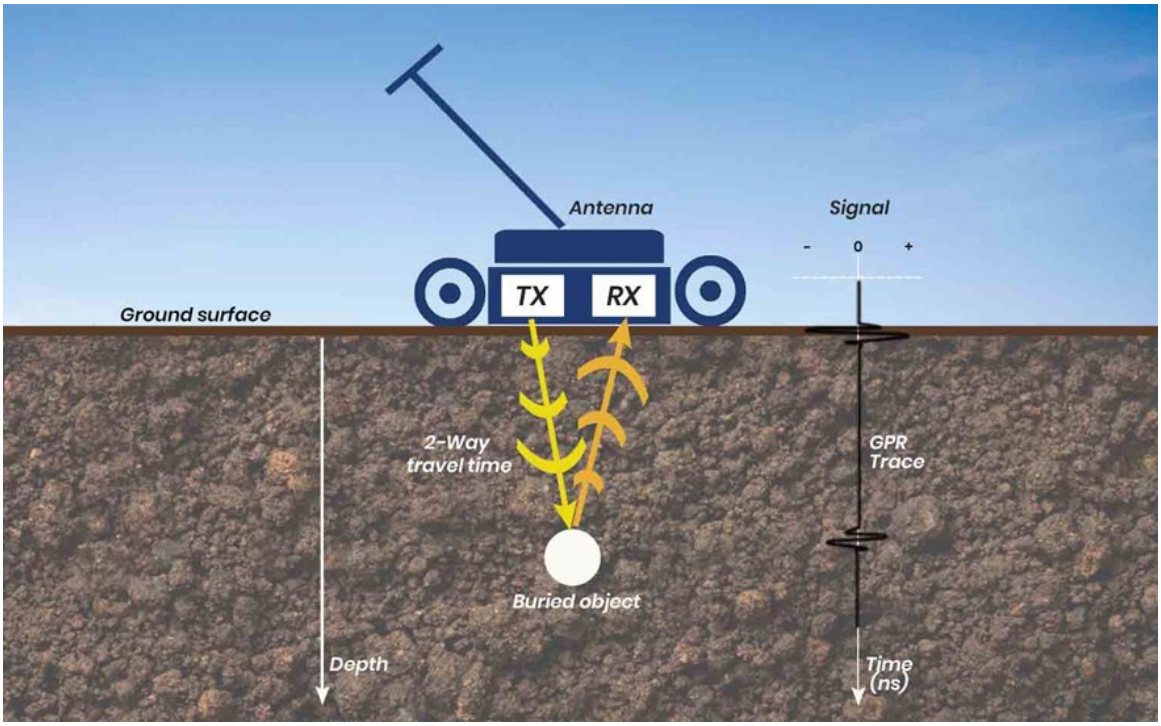

Figure 2.1: *Display of the monostatic Ground Penetrating Radar (GPR) method (https://impulseradargpr.com/technology/).*

The GPR system consists of a signal generator, transmitting and receiving antennas, and an analog or digital recorder with graphic display capabilities. GPR works by emitting pulses of high frequency radio waves in a spectrum from 10 MHz to 1 GHz. This energy is emitted by an antenna (transmitter) on the ground in the form of lobes and as it propagates in space it comes into contact with objects or interfaces with different electromagnetic properties. Part of the energy is reflected to the surface, while the rest continues its course in the propagating medium until it encounters the next change in electromagnetic properties. The energy reflected to the surface is received by the antenna (receiver). The received signal is then amplified and recorded with respect to the two-way travel time by the recorder. For each reflected wave the signal received by the GPR changes polarity two times. The inhomogeneity of the material in which the energy is propagated is the main factor that determines the number of reflections that will be received 9 (fig.2.1).

GPR systems can either be **shielded** or **unshielded** and are divided into two categories depending on the functionality of the antenna (fig. 2.2):

- Monostatic systems: A single antenna functions as a transmitter and a receiver at the same time (transmits – switches mode – receives / records etc.)
- Bi-static systems: The transmitter and the receiver are separate antennas.

Figure 2.2: *Left image depicts a shielded monostatic GPR antenna and the right image depicts an unshielded bistatic GPR antenna.*

The operating principle of the antenna affects the geometry that the signal is emitted. In the shielded antenna the signal-pulse is emitted in the form of a "cone", while in the unshielded one as a "hemisphere".

2.1 Electromagnetic Theory

Applications of the Ground Penetrating Radar method are quick and practical, but the signals corresponding to the GPR depend on a multitude of physical properties. Therefore, it is beneficial to have a basic understanding of the fundamental physics that the GPR functions upon.

2.1.1 Maxwell's equations

In order to use Electromagnetism in the geophysical investigation of the Earth's interior, first we have to understand its basic principles. Maxwell's equations mathematically describe the physics of EM fields.

$$\nabla \times \mathbf{H} = \mathbf{J} + \frac{\partial \mathbf{D}}{\partial t} \quad (1)$$

$$\nabla \times \mathbf{E} = -\frac{\partial \mathbf{B}}{\partial \mathrm{t}} \quad (2)$$

$$\nabla \cdot \mathbf{B} = 0 \quad (3a)$$

$$\nabla \cdot \mathbf{D} = \rho \quad (3b)$$

Equation 1 is Ampère's Law, which describes the fact that electric current flow in a conductor, produces a magnetic field. ***H*** is the magnetic field strength in *A/m*, ***J*** is the current density in A/m^2 and ***D*** is the dielectric shift in Cb/m^2.

This equation includes two types of electricity.

Equation 2 is Faraday's law, which describes the fact that the magnetic induction within an electrically conductive medium induces an electric field and an electric current within the medium. ***B*** is the magnetic induction in Wb/m^2 and ***E*** is the electric field strength in *V/m.*

Finally, Gauss's two laws are listed. *(Equation 3a and Equation 3b)*

Gauss's law of magnetism says that the total magnetic field flux through a closed surface is zero, i.e. no magnetic field is produced inside that surface. Gauss's law for electricity is given in the special

form which says that the total flow of electric field through a closed surface is zero, i.e. there are no sources of electric field and current inside this surface (space free of electric sources or consumers).

2.1.2 Constitutive relationships

For electromagnetic geophysical investigations, the electrical and magnetic properties are of importance. Constitutive relationships are the means of describing a material's response to EM fields.

$$J = \sigma E \qquad (4)$$

$$D = \varepsilon E \qquad (5)$$

$$B = \mu H \qquad (6)$$

- Electrical conductivity **σ** characterizes free charge movement (creating electric current) when an electric field is present. Resistance to charge flow leads to energy dissipation.
- Dielectric permittivity **ε** characterizes displacement of charge constrained in a material structure to the presence of an electric field. Charge displacement results in energy storage in the material.
- Magnetic permeability **μ** describes how intrinsic atomic and molecular magnetic moments respond to a magnetic field. For simple materials, distorting intrinsic magnetic moments store energy in the material.

For GPR, the dielectric permittivity is an important quantity. Most often, the terms relative permittivity or dielectric constant (**κ**) are used and defined as follows:

$$\kappa = \frac{\varepsilon}{\varepsilon_0} \qquad (7)$$

Where $\boldsymbol{\varepsilon}$ is the permittivity of the material and $\boldsymbol{\varepsilon_0}$ is the permittivity of vacuum, $8.854 \times \frac{10^{-12} F}{m}$.

In most GPR applications, variations in **ε** and **σ** are most important while variations in **μ** are rarely of concern.

2.1.3 Electromagnetic waves

Ground penetrating radar exploits the wave character of EM fields. Maxwell's equations describe a coupled set of electric and magnetic fields when the fields vary with time. Depending on the relative magnitude of energy loss (associated with conductivity) to energy storage (associated with permittivity and permeability), the fields may diffuse or propagate as waves. Ground penetrating radar is viable when conditions yield a wave-like response**.**

The wave character becomes evident when Maxwell's equations are rewritten to eliminate either the electric or the magnetic field. Using the electric field, rewriting yields the transverse vector wave equation:

$$\nabla \times \nabla \times E + \mu\sigma \cdot \frac{\partial E}{\partial t} + \mu\varepsilon \cdot \frac{\partial^2 E}{\partial t^2} = 0 \qquad (8)$$

Ground penetrating radar is effective in low-loss materials where energy dissipation ($\boldsymbol{\mu\sigma \cdot \frac{\partial E}{\partial t}}$) is small compared to energy storage ($\boldsymbol{\mu\varepsilon \cdot \frac{\partial^2 E}{\partial t^2}}$).

2.1.4 Propagation of radio waves

The reflections recorded by a GPR system measure the travel time from the emission of the signal to the reflector and the return time to the receiving antenna. The speed (V) with which energy is propagated in a medium is given by the relation:

$$V = \frac{c}{\sqrt{\frac{\varepsilon_r \mu_r}{2}\left[\left(\sqrt{1+P^2}\right)+1\right]}}$$

- **c** the speed of light in vacuum ($3 \cdot 10^8$ m/s ή 0.3m/ns),
- $\boldsymbol{\mu_r}$ relative magnetic permeability **which is approximately equal to 1 for non-magnetic rocks**,
- **P** loss factor (P = σ/ωε), where **σ** the conductivity and ω=2πf,
- **ε**= $\varepsilon_r\varepsilon_0$ the dielectric permittivity, $\boldsymbol{\varepsilon_0}$ the dielectric permittivity in vacuum ($8.854 \cdot 10^{-12}$ F/m) and $\boldsymbol{\varepsilon_r}$ the relative permittivity of the rock.

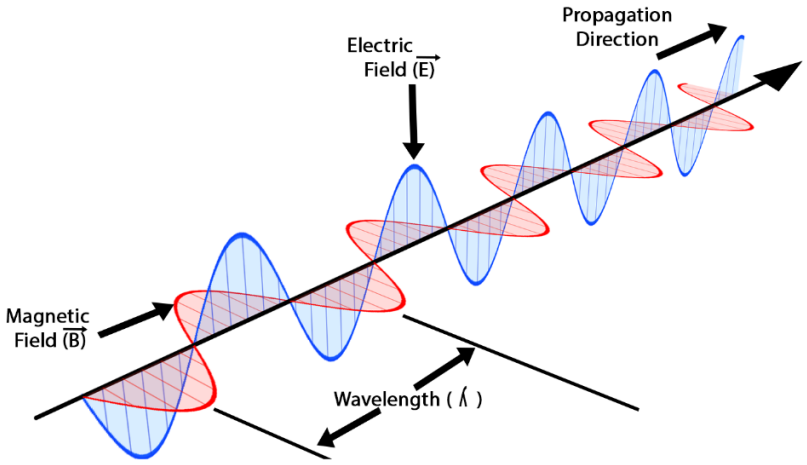

Figure 2.3: *Image depicting the propagation of an electromagnetic wave (https://www.toppr.com/guides/physics/communication-systems/propagation-of-electromagnetic-waves/).*

For propagation medium with paramagnetic properties $\boldsymbol{\mu_r=1}$ and low loss/low attenuation, we consider **P**≈ **0** the equation becomes:

$$V = \frac{c}{\sqrt{\varepsilon_r \mu_r}} = \frac{c}{\sqrt{\varepsilon_r}}$$

From the previous expression, we can see that radiowaves propagate more slowly in increasingly dielectric materials (Table 1).

Table 2.1: Approximate dielectric permittivities, electrical conductivities and radiowave velocities for various materials.			
Material	**Relative Permittivity**	**Conductivity (mS/m)**	**Average Velocity(m/ns)**
Air	1	0	0.3
Fresh Water	80	0.5	0.033
Sea Water	80	3000	0.01
Ice	3-4	0.01	0.16
Dry Sand	3-5	0.01	0.15
Saturated Sand	20-30	0.1-1	0.06
Limestone	4-8	0.5-2	0.12
Shales	5-15	1-100	0.09
Silts	5-30	1-100	0.07
Clays	5-40	2-1000	0.06
Granite	4-6	0.01-1	0.13
Anhydrites	3-4	0.01-1	0.13

2.1.5 Attenuation

Attenuation defines the continuous loss of amplitude a wave experiences as it propagates through a particular medium. The rate at which the amplitude decreases is referred as the attenuation constant (***α***) (fig. 2.4). For an electromagnetic wave that has traveled a distance ***z***, the attenuation constant is given by:

$$\frac{|A|}{|A_0|} = e^{-az}$$

where $\boldsymbol{A_0}$ is the initial amplitude of the wave and **A** is the amplitude of the wave after it has travel distance ***z***. We can see that as $z \to \infty$ the amplitude of the wave goes to zero. Additionally, for larger values of **α**, the wave attenuates more quickly.

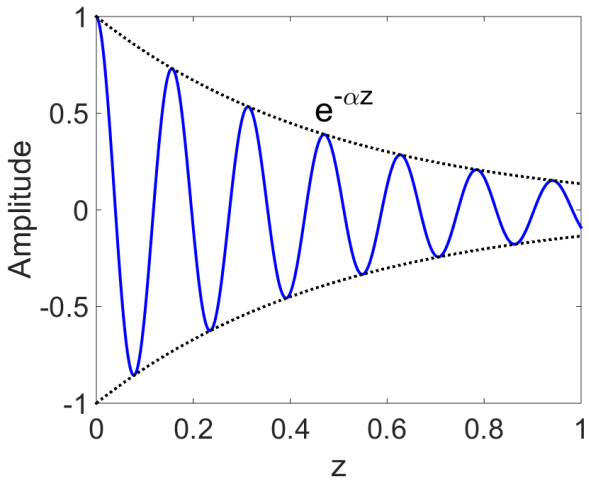

Figure 2.4: Attenuation of electromagnetic waves (https://gpg.*geosci*.xyz/content/GPR/GPR_fundamental_principles.html).

The attenuation constant depends on the physical properties of the media. In general, the attenuation constant can be expressed as:

$$\alpha = \omega \sqrt{\frac{\varepsilon\mu}{2}\left[\sqrt{\left(1+\left(\frac{\sigma}{\omega\varepsilon}\right)^2\right)}-1\right]}$$

GPR signals are characterized as being high-frequency. Thus in many cases, it is safe to assume that $\sigma \ll \omega\varepsilon$ and therefore the equation is simplified to:

$$\alpha = \frac{\sigma}{2}\sqrt{\frac{\mu}{\varepsilon}}$$

The attenuation of radiowaves occurs due to various factors, such as:

- Geometrical Spreading
- Scattering from small inhomogeneities (reflectors).
- Attenuation (conversion to thermal energy).
- Antenna losses.

The detectability of underground targets depends on:

- The power and frequency of the transmitter
- The nature of the target
- The loss of energy

2.1.6 Skin Depth

Skin depth (δ) defines the propagation distance at which the amplitude of an electromagnetic wave is reduced by a factor of $1/e$ (37%) of its original amplitude. By definition, the skin depth is just the reciprocal of the attenuation constant (Jol, 2009) (fig. 2.5):

$$\delta = \frac{1}{a}$$

If we use the same approximations as we did previously and assume the Earth is non-magnetic ($\mu_r = 1$), the skin depth is given by:

$$\delta = \frac{5.31\sqrt{\varepsilon_r\omega}}{\sigma}$$

Generally, the skin depth is smaller if the frequency of the electromagnetic waves is higher.

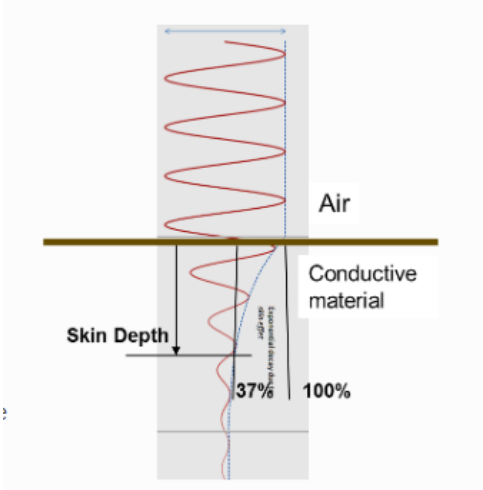

Figure 2.5: *Attenuation of radiowaves in the air versus in a conductive medium (https://gpg.geosci.xyz/content/GPR/GPR_fundamental_principles.html).*

2.1.7 Reflection of Radiowaves

When a radiowave reaches an interface, a part of the energy is reflected. The amplitude of the reflected wave is proportional to that of the incident wave and is defined by the reflection coefficient (R). For radiowaves, the reflection coefficient is expressed as a function of the **relative permittivities** on each side of the interface. Assuming the radiowave interacts at an angle perpendicular to the interface, the reflection coefficient can be given by:

$$R = \frac{V_2 - V_1}{V_2 + V_1} = \frac{\sqrt{\varepsilon_1} - \sqrt{\varepsilon_2}}{\sqrt{\varepsilon_1} + \sqrt{\varepsilon_2}}$$

where V_1 and V_2 are the velocities in the layers 1 and 2 respectively and ε_1 and ε_2 are their dielectric constants.

The reflection coefficient can be either positive or negative and has values between $-1 < R < 1$. The magnitude of R determines how much of the incident wave is reflected.

- If ε_1 and ε_2 are similar, the majority of the incident wave is transmitted through the interface.
- If one of the relative permittivities across the interface is much smaller in regards to the other, most of the incident wave will be reflected. This can cause a problem if the goal is to gain information about structures below this interface.

The sign of the reflection coefficient determines whether the reflected wave experiences a reverse in polarity. As a result, we can use the polarity of reflected radiowaves to determine whether ε_1 is greater than or less than ε_2.

- If the returning signal (reflected wave) shows a reverse in polarity, $R < 0$ and thus $\varepsilon_1 < \varepsilon_2$
- If the returning signal (reflected wave) does not show a reverse in polarity, $R > 0$ and thus $\varepsilon_1 > \varepsilon_2$

2.1.8 Refraction of Radiowaves

Refraction is used to describe the change in propagation direction of a wave due to a change in the propagation medium. When a radiowave reaches an interface, recall that some of it is reflected and some of it is transmitted across the interface.

The angle of the reflected portion depends directly on the angle of the incident wave. The angle of the refracted wave can be obtained by using Snell's law:

$$\frac{\sin\theta_1}{V_1} = \frac{\sin\theta_2}{V_2}$$

For radiowaves in resistive and non-magnetic media, the propagation velocity is equal to $V = c/\sqrt{\varepsilon_r}$. In this case, Snell's law can be expressed as:

$$\sqrt{\varepsilon_1}\sin\theta_1 = \sqrt{\varepsilon_2}\sin\theta_2$$

2.1.9 Critical Refraction and reflection of radiowaves

Radiowaves can undergo critical refractions and reflection (fig. 2.6). This occurs when the incident angle $\theta_1$is such that the refracted wave propagates along the interface at velocity V_2; ultimately leading to a head wave. The critical angle (θ_c) is given by:

$$sin\theta_c = \frac{V_1}{V_2}$$

Once again, we can see that critical refraction only occurs when $V_1 < V_2$. Additionally, the propagation direction of the head wave is characterized by θ_c.

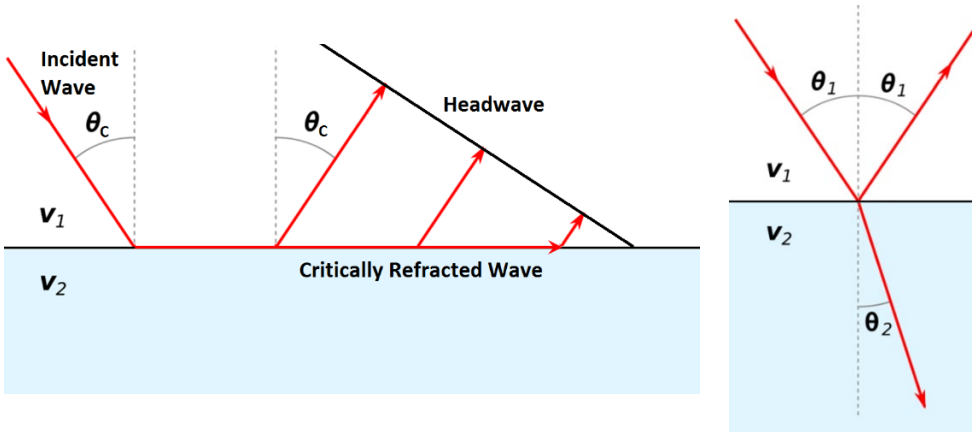

Figure 2.6: *Left figure depicts critical refraction at an interface and the resulting head-wave. Right figure depicts the reflection and refraction of an incident radiowave. (*https://gpg.geosci.xyz/content/GPR/GPR_fundamental_principles.html).

2.1.10 Survey Resolution

The pulse width, and thus the frequency content contained within the GPR signal, is a very important aspect of planning a GPR survey.Vertical Resolution

Resolution defines the smallest features which can be distinguished in a GPR survey. The vertical resolution for GPR surveys depends on the pulse width of the signal. In order for a layer to be

detected using a GPR survey, it must be sufficiently thick compared to the wavelength of the incoming wavelet. As a general rule, the layer must be at least 1/4 the wavelength of the incoming wavelet to be detectable. Thus:

$$L > \frac{\lambda}{4} = \frac{c}{4f_c\sqrt{\varepsilon_r}} = \frac{c\Delta_t}{4\sqrt{\varepsilon_r}}$$

where L is the layer thickness, $c/\sqrt{\varepsilon_r}$ is the propagation velocity for radiowaves, Δ_t is the pulse width and f_c is the central frequency. As we can see from this expression, **higher frequencies/shorter pulse widths are required to observe smaller features**. This means **higher frequencies/shorter pulse widths are used for higher resolution surveys.**

Horizontal Resolution

When the resolution of the survey is sufficient, returning signals from separate buried objects are distinguishable. However, if buried objects are too close to one another, their respective returning GPR signals can be hard to differentiate. In general, we can distinguish the signals from two nearby objects so long as:

$$L > \sqrt{\frac{Vd}{2f_c}}$$

GPR data can be presented in various ways, the main ones being one-dimensional (1D) traces, two-dimensional (2D) sections and three-dimensional (3D) representations (Annan, 2009; Conyers, 2013), (figs 2.7, 2.8) which based on the terminology of acoustics can be named respectively as:

1. A-scan, Amplitude scan
2. B -scan, Brightness scan
3. C-scan, Contrast scan (Volume/depth slices)

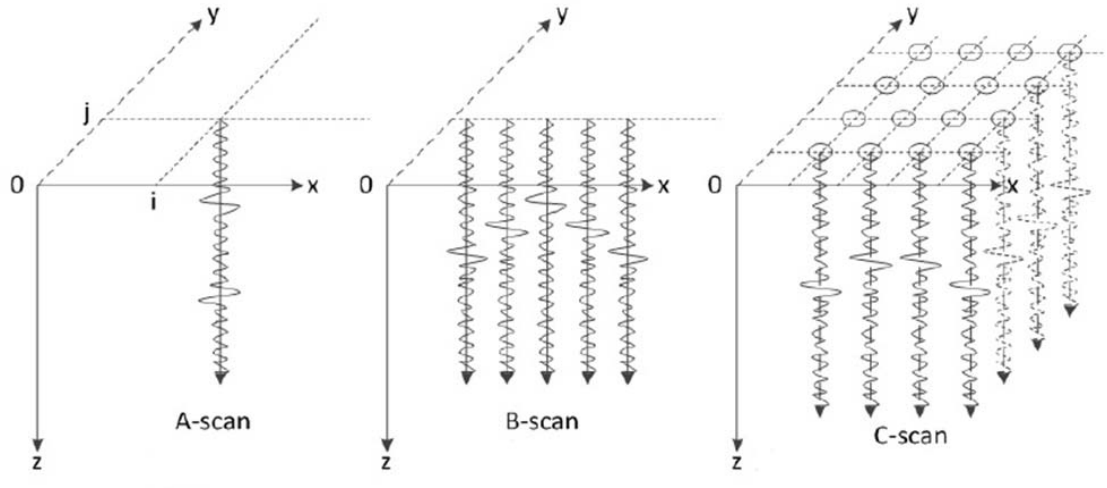

Figure 2.7: *Different ways to present the results of GPR data (Conyers, 2013).*

The **one-dimensional trace** (A-scan) refers to a single point on the surface, which represents the amplitude of the signal amplitude as a function of the two-way travel time of the electromagnetic wave corresponding to the depth. On the horizontal axis the intensity and polarity of the signal is recorded and on the vertical the time.

Two-dimensional slices (B-scans) are derived from the individual one-dimensional traces (A-scans) collected along the antenna path. The acquired data can be visualized through the use of a predefined color scale, matching the strength of the recorded signal to a specific hue of the palette selected. This image, also referred to as a radargram (B-scan), represents a vertical cross section on the ground, where the horizontal axis corresponds to the position of the antenna along the scan (distance) and the vertical axis to the two-way travel time electromagnetic wave corresponding to depth.

The **three-dimensional images** (C-scan) are produced from the collection of multiple parallel two-dimensional sections (B-scans) in the form of a grid (fence diagram). For the visualization of 3D results, the use of a properly designed grid is required, so that the necessary number of measurements are collected properly, which will create the three-dimensional display with as little uncertainty as possible and without the fear of creating artifacts.

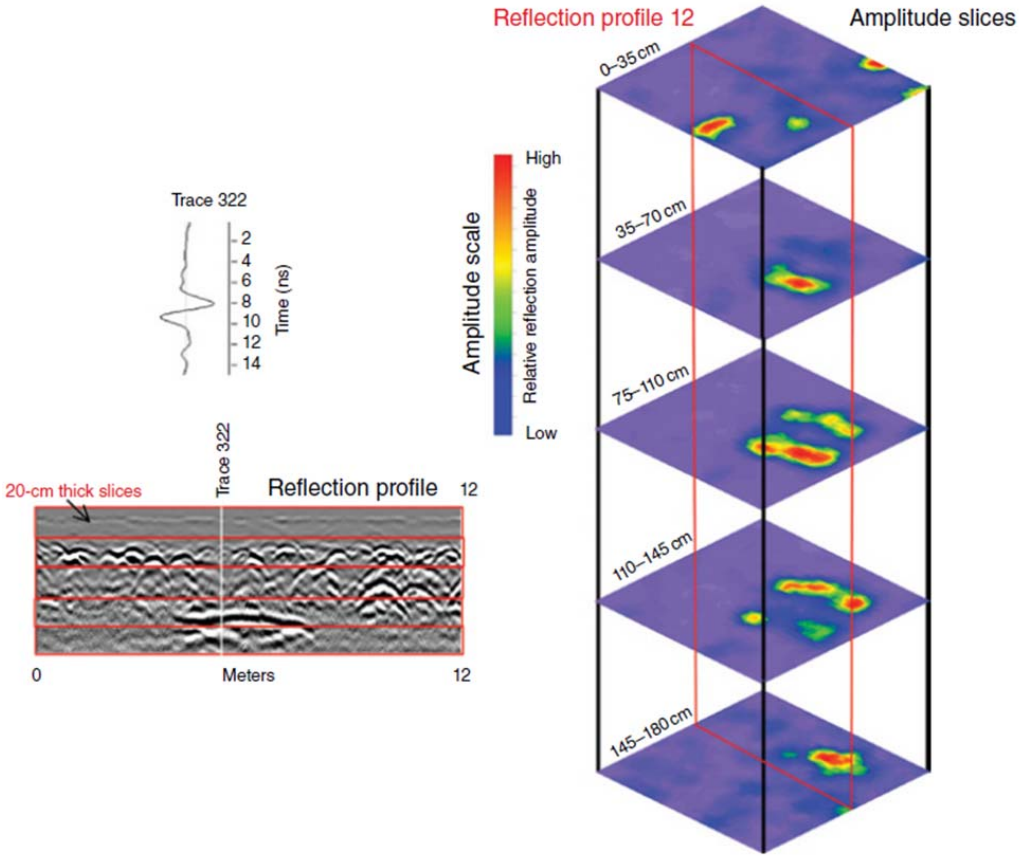

***Figure 2.8**: The production of GPR images, beginning with individual traces from one location on the ground, stacked together to produce reflection profiles, with an additional product being amplitude slice-maps of resampled reflection trace amplitudes in individual maps from programmed depths in the ground (Conyers 2013).*

2.2 Data analysis

Transforming GPR data into useful information for our investigations is a strenuous process that can follow many paths. A typical processing flow for GPR data is depicted in figure 2.9.

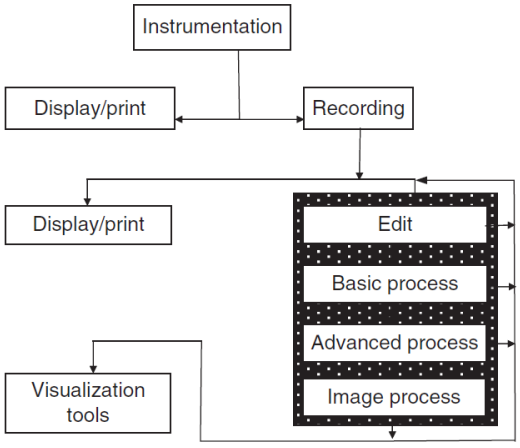

Figure 2.9: *Overview of ground penetrating radar (GPR) data processing flow (Jol, 2009).*

Processing can vary, starting from simple editing to total transformation of the GPR data into different forms. The main processing steps that are commonly used for GPR data, are very similar to those of seismic reflection analysis and consist of:

I. The Data Editing
II. The Basic Processing
III. The Advanced Data Processing
IV. The 2D & 3D Interpretation

The data processing flow is an iterative process, which is first applied to a part of the data and then to the whole volume.

Data Editing

From the moment the data is recorded, the first processing stage is of great importance. This is due to the fact that the data acquisition is a procedure which does not accept errors and data redundancy. This processing includes steps such as data reorganization, file merges, headings and history refreshing, placement of measurements in their real coordinates. All of these might seem like they have little effect in the final results, but when we are dealing with large amounts of data, overlooking this step can cause our results to deviate leading us to false interpretations.

2.3 Processing methods

After any geophysical survey has been conducted, the raw data that has been acquired from the field rarely can be used as it. This is especially true for GPR data where various factors can affect them, making it difficult to yield clear results. In order to make the data more manageable and increase the Signal to Noise ratio, several processing methods are commonly utilised.

2.3.1 Velocity analysis and conversion of travel time to depth

The data measured by the GPR system is the amplitude of the signal as a function of its two-way travel time. However, interpretation can be made easier if the information can be represented in

terms of depth. To convert the two-way travel time to apparent depth, we must choose a propagation velocity.

This may be acquired from the initial radargram, from a-priori information, or sometimes left as the speed of light ($c = 3.00 \times 10^8\ m/s$). The conversion is given by:

$$d_a = \frac{V_t}{2}$$

where d_a is the apparent depth, V is the propagation velocity and t is the two-way travel time.

2.3.2 Time-zero correction

In GPR surveys it is necessary to have a fixed reference as a time-zero point for the GPR data, in order to compare the reflection time and the depth of inhomogeneities located at different positions along the survey track. Mostly, this cannot be ensured due to several factors, such as the different temperature of the air during the collection of the data, the different length of the connecting cables or, more simply, the variation of the antenna height due to the vertical acceleration acting on the instrumented vehicle. To avoid interpretation issues arising from a variable time-zero reference, the data need a correction to set a common time-zero position. This issue can be sorted by cutting the air layer to a fixed threshold, set at a mostly stable point of the considered trace. Depending on both the type of the antenna and the central frequency of investigation, setting the proper position of this threshold reflects on the accuracy of the results. The possible thresholds that are often employed by users and advised by manufacturers can be summarized as:

- the first break-point
- the first negative peak
- the zero-amplitude point between the negative and the positive peaks
- the mid-amplitude point between the negative and the positive peaks
- the first positive peak

Each method holds advantages and drawbacks regarding the dielectric properties of the surface materials and the central frequency of investigation.

2.3.3 Zero offset removal

The initial direct current (DC) signal component and the very low-frequency signal trend (or 'wow') can generate a distortion towards values of amplitude far from zero. This occurrence is partially related to the coupling effect and to the saturation of the signal by early arrivals. It can affect the spectrum of the trace and inhibit further spectral processing steps. Mostly, processing software are capable to sort out this problem by using simple average-subtraction algorithms, such as the following:

$$y'(n) = y(n) - \frac{1}{N}\sum_{k=1}^{N} y(k)$$

with $y(n)$and $y_r(n)$being the amplitude of the n^{th} sample of the processed and raw trace, respectively, and with n ranging from 1 to N. The result of the application of this algorithm turns out

to be an A-scan with mean equal to zero, which means a symmetric probability distribution of the amplitude along the A-scan (fig. 2.10).

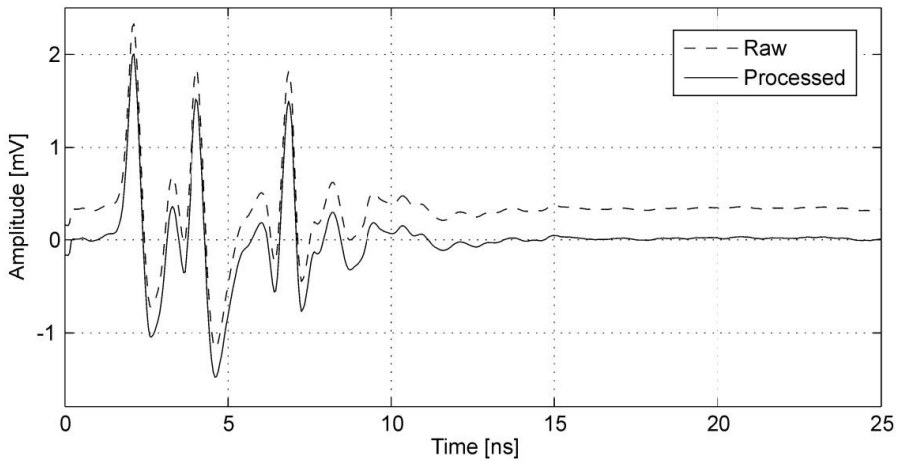

Figure 2.10: *Application of the Zero offset removal processing method (Benedetto et al. 2016).*

2.3.4 Time gain

Due to the dispersive nature of the EM wave and to the geometrical spreading losses, the GPR signal suffers from attenuation when propagating through a medium. The intensity of such attenuation is related to the electrical conductivity of the medium. Mostly in case of high conductivity materials, such as clayey soils, deeper targets can be hardly detected. It can be worth to compensate the loss suffered by the signal when applying a time-varying gain to each A-scan

The spherical and exponential (SEC) function operates by compensating the loss of energy caused by geometrical spreading effects, with an exponential relationship. On the other hand, the automatic gain compensation (AGC) works by sorting each signal trace in several time windows characterized by different average amplitudes. The compensation applied by the algorithm is a function of the difference between the average amplitude within a time window and the maximum amplitude of the whole trace. In this case, the width of the time windows highly influences the performances of the process. As a rule of thumb, simple constant, linear or exponential gain functions can be applied to the signal, at the discretion of the user (fig 2.11). Nevertheless, **the choice of the type of gain function should depend on the physical model of the target.**

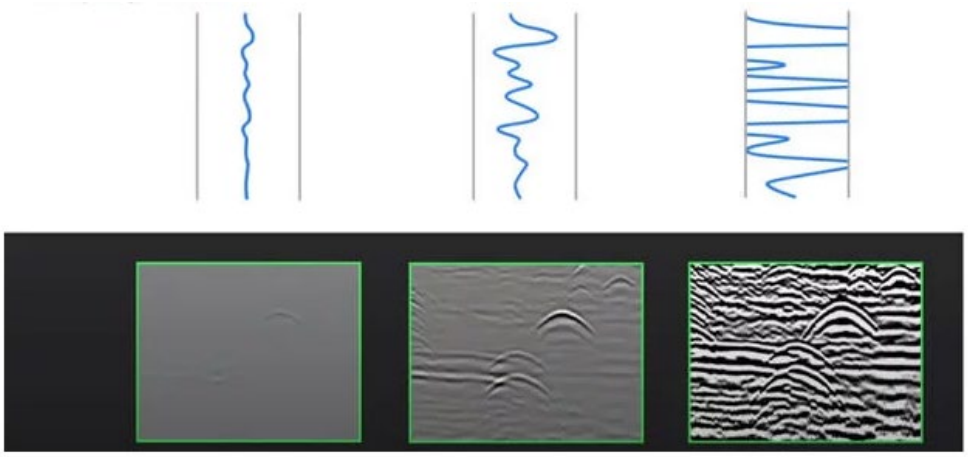

Figure 2.11: *Same data set is shown at three different gain levels. Left, the data displayed is "under gained." Right, the data is "over gained." The properly gained signal is displayed by the center image (https://www.geophysical.com/gssi-academy-how-to-bring-out-gpr-targets-more-clearly-using-gain).*

2.3.5 Background removal

This method relies on the fact that reflections recorded at the same time in a profile, which exhibit the same wave "signature" within a running series of traces, will have likely been generated by background noise that obscures reflected waves generated from within the ground. It creates a composite trace of waves that were recorded in all or some number of sequential traces in a profile and then removing that average trace from each trace within the profile. That background noise can then be removed from all the reflections in a profile(fig.2.12), retaining and displaying only those that were obtained from within the ground and were likely to have been recorded at different times and with different amplitudes. In most cases this simple procedure creates a much "cleaner" reflection profile where only those reflections of interest are displayed. However, there is a somewhat low risk that perfectly horizontal reflections from some interface in the ground could be removed by this procedure. Usually once background waves are removed, profiles must again be re-gained in order to visualize the remnant reflections of interest in a profile.

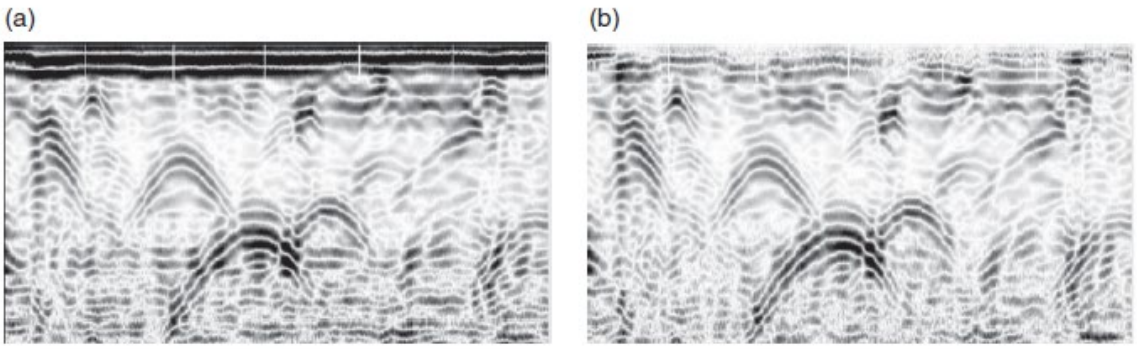

Figure 2.12: *Application of the background removal filter on GPR data. Left image (**a**) depicts the raw data and the right image (b) depicts the data after the filter has been applied. (Jol, 2009).*

2.3.6 Bandpass filtering

The application of a band-pass filter (fig.2.13) may represent a crucial step for a correct visualization and interpretation of a GPR signal. This processing method is aimed at increasing the Signal to Noise Ratio (SNR) by filtering out from the data the signal components with frequencies outside the main working bandwidth of the GPR system employed. A band-pass filter can be considered as the combination of two frequency filters, the **high-pass** and the **low-pass** filters. The first one operates a cut-off of the low frequency components from the frequency spectrum of each singular trace. This allows to filter the clutter related to both the ground-wave and the other sources of noise, such as nearby vehicles, buildings, fences, power lines or trees in close proximity to the roadway. The low-pass filter works by cutting off the high frequency components from the spectrum, which are usually generated by the EM interferences between the antenna and relevant everyday EM devices, such as mobile phones.

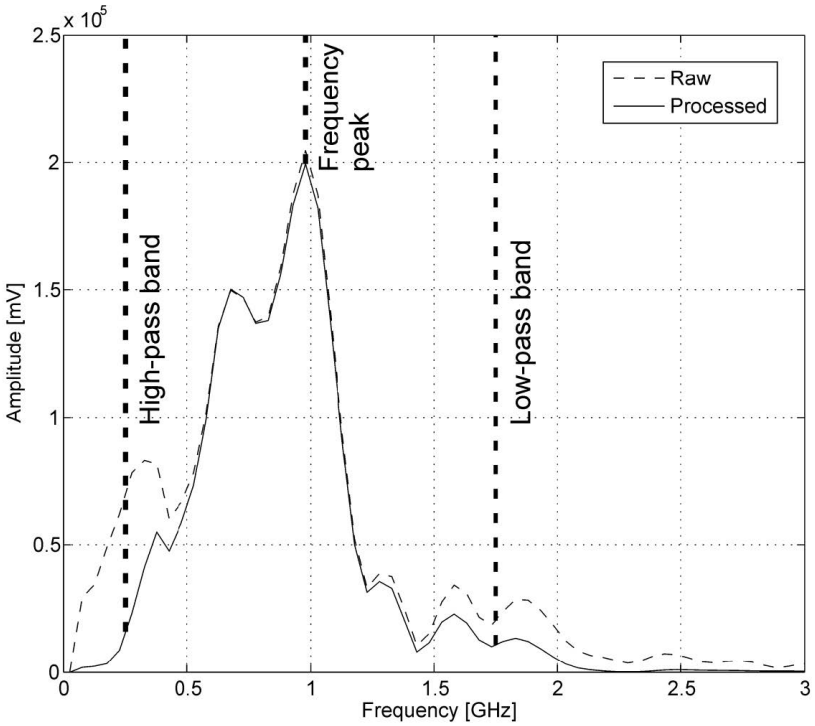

Figure 2.13: *Bandpass filtering in the frequency spectrum of a GPR signal (Benedetto et al. 2016).*

2.3.7 Migration

Migration is a basic data processing step that can move radar reflections to a more accurate location in a reflection profile. A distortion on the position of the reflections can be caused by radar waves that have moved into the ground in a conical transmission pattern and are then recorded in a location not directly below the surface antenna. The most common of these distorted reflections are hyperbolas generated from individual “point sources.” The migration processing step can enhance the amplitudes generated at the apex of reflection hyperbolas, while removing their axes. To perform this step, velocity estimates of the ground must be determined so that hyperbolas can be affectively removed, as their geometry is a function of velocity. This is always difficult, as in most ground conditions, velocity changes with depth (usually slowing) and also varies laterally. A velocity that

might be used for all hyperbolic reflection migrations can over or under-migrate many, sometimes producing very blurred or distorted reflection profiles. Migration can be a particularly beneficial processing step prior to producing amplitude slice-maps, as migrated profiles will be much more "crisp" and less distorted by ***hyperbolas*** (fig.2.14). Migration is also a processing step that can be used to correct steeply dipping layers that are distorted by radar wave movement in a non-vertical path from the surface antenna.

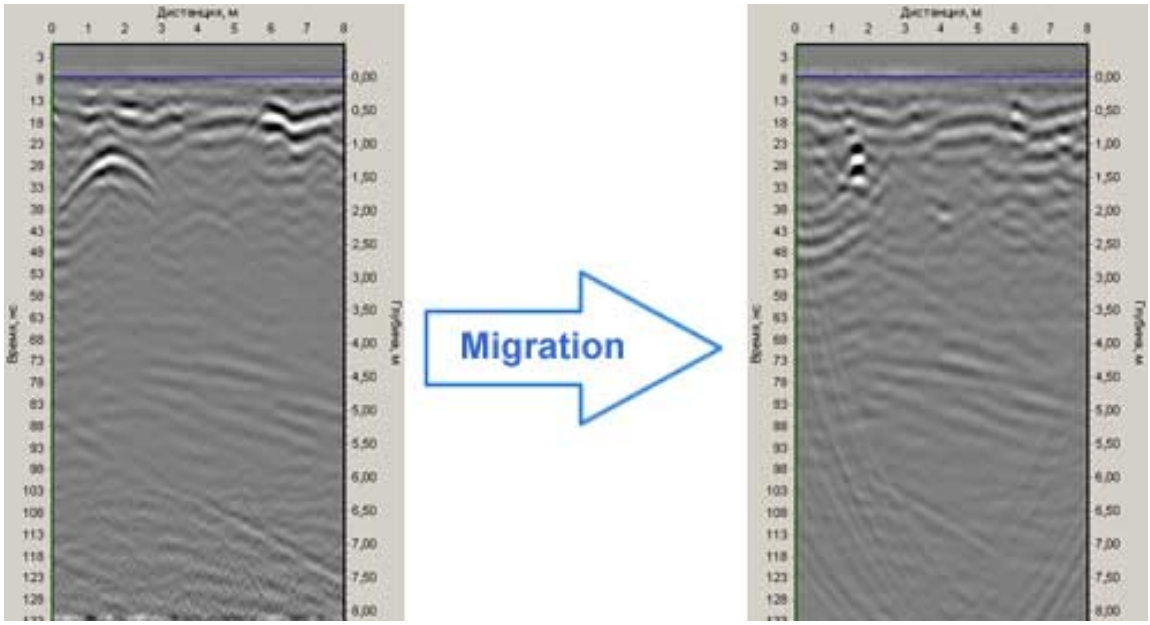

Figure 2.14: *Application of Migration correction on GPR data. Left image depicts the data before the Migration has been applied and the right image after the Migration has been applied. (https://viy.ua/e/news/20130822161153.htm).*

3. GPR software and data processing

The goal of most GPR investigations is to discover what lies beneath the ground. After the data acquisition is done, all the raw data that is gathered cannot give us a clear perspective of our goal. Thus, for a proper interpretation to be done, we have to process the data accordingly. For this reason, a plethora of processing software has been developed and upgraded over the years. In this thesis the software that has been used is MALÅ Vision from GuidelineGeo.3.1. MALÅ Vision

MALÅ Vision is a cloud-based software that can be used for analysis, processing and interpretation of GPR data. For this thesis, in order to achieve the desirable results, the following steps were taken.

Firstly, due to the fact that the software is cloud-based, internet connection is required to log in to our account. After that, we will be redirected to the following window (fig. 3.1).

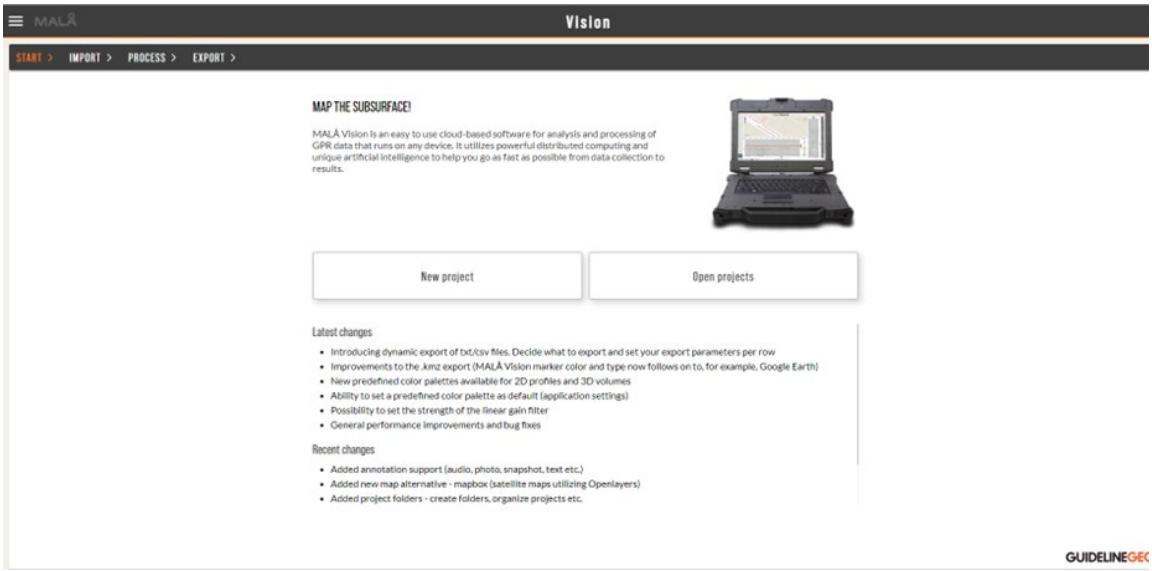

Figure 3.1: *Image taken from MALÅ Vision software, depicting its initial user interface.*

From there, we can either create a new project or open an existing one by left clicking on the necessary option.

By creating a new project, we are then prompted to another window, where the software allows us to name the project and also input the files that are going to be processed for the current project. To upload the files, we can either use the browse function or we can just drag the files from their initial location and drop them onto the MALÅ Vision window (fig.3.2).

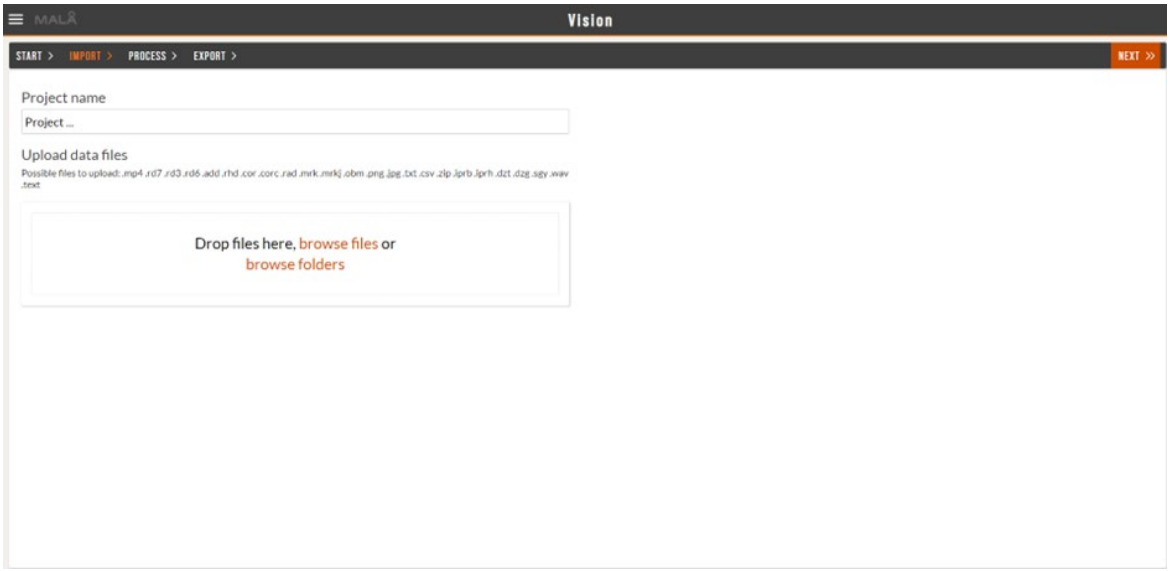

Figure 3.2: *Image taken from MALÅ Vision depicting the interface where the GPR data can be uploaded.*

After all the necessary data has been selected, we click on the **Upload Files** button to start uploading them. The upload progress can be viewed in the Import tab for each file. The upload progress is clearly seen in the Import tab for each file and when it is ready, the file gets a green tick mark (fig. 3.3).

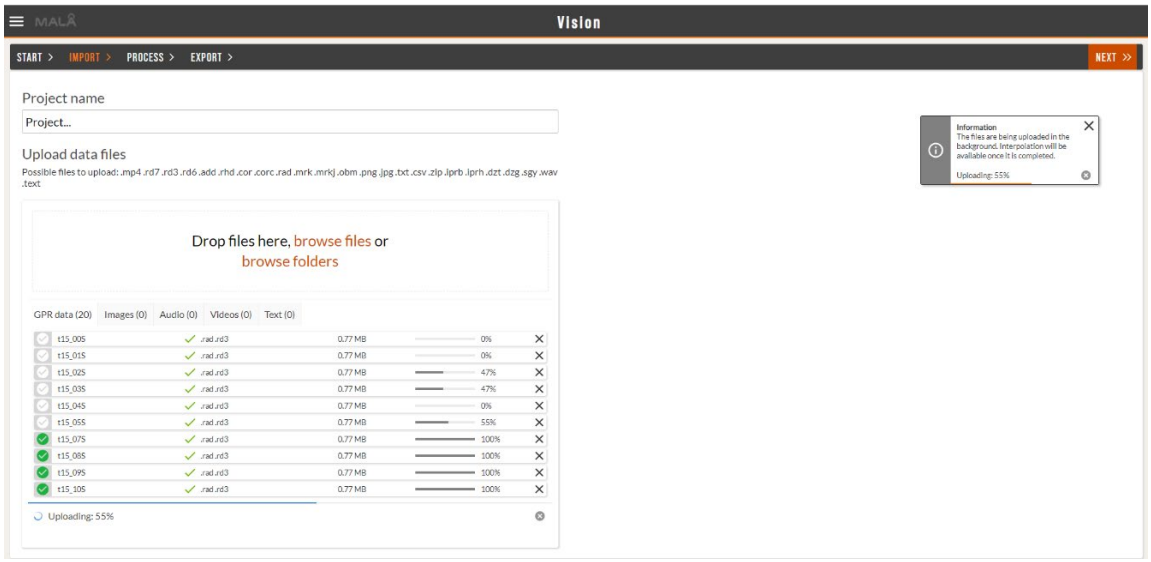

Figure 3.3: *Image taken from MALÅ Vision depicting the uploading process.*

When everything needed is uploaded, each GPR data file will be displayed in 2D mode. A list of all the imported GPR profiles can be found under the panel to the left side of the window. If we press the arrow on the left side, we can view and navigate between the imported profiles. On the right side of the panel, there are various tools to use for analysis, processing and interpretation.

3.1 Data processing

To achieve the desirable results, the following steps were carried out:

Firstly, using the analysis option and turning on the trace view, we can choose to display a single trace or an average trace for the whole profile. Because of the inhomogeneity of the area that is

being investigated, choosing to work only with a single trace would make the processing more difficult due to the fact that the trace would change its characteristics through the profile. Thus, choosing to display the average trace for the whole profile is the more beneficial option. After that, using the ***Filters*** option we click on the ***Add filter*** button and select **DC Offset** (fig. 3.4).

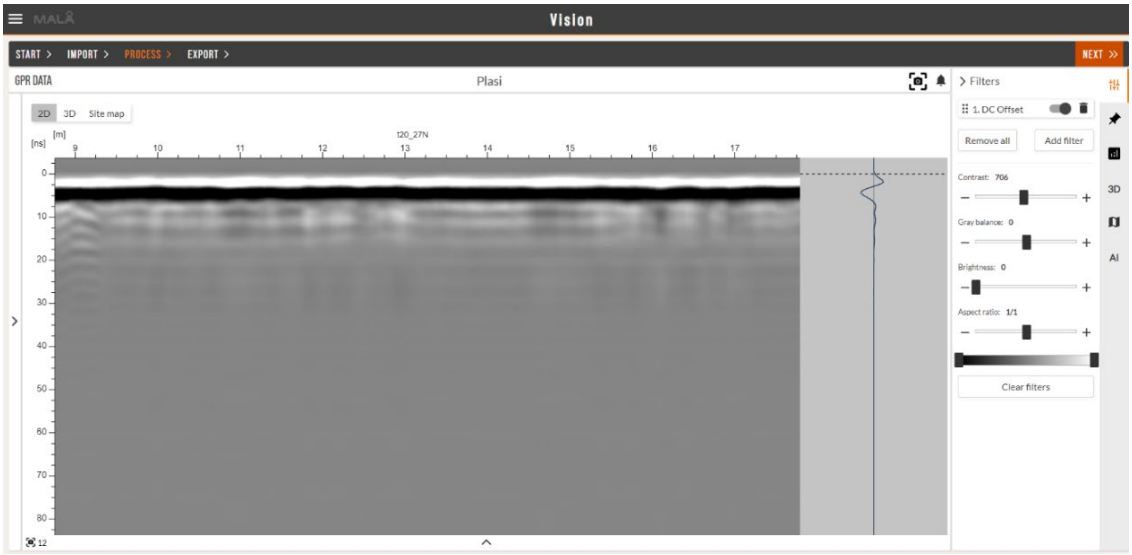

Figure 3.4: Image showing the application of DC offset filter. (MALÅ Vision software)

As it is mentioned before see (1.2.2), due to several factors GPR data need to have a fixed **time-zero point**, in order to compare the reflection time and the depth of inhomogeneities that are located at different positions throughout the survey track. For this to be done, we need to choose the analysis button and under the Set time zero option we can either choose to do so manually or let the software do it automatically. For the purposes of this investigation time zero correction was chosen to be done manually be selecting the **first break-point** from the average trace (fig. 3.5).

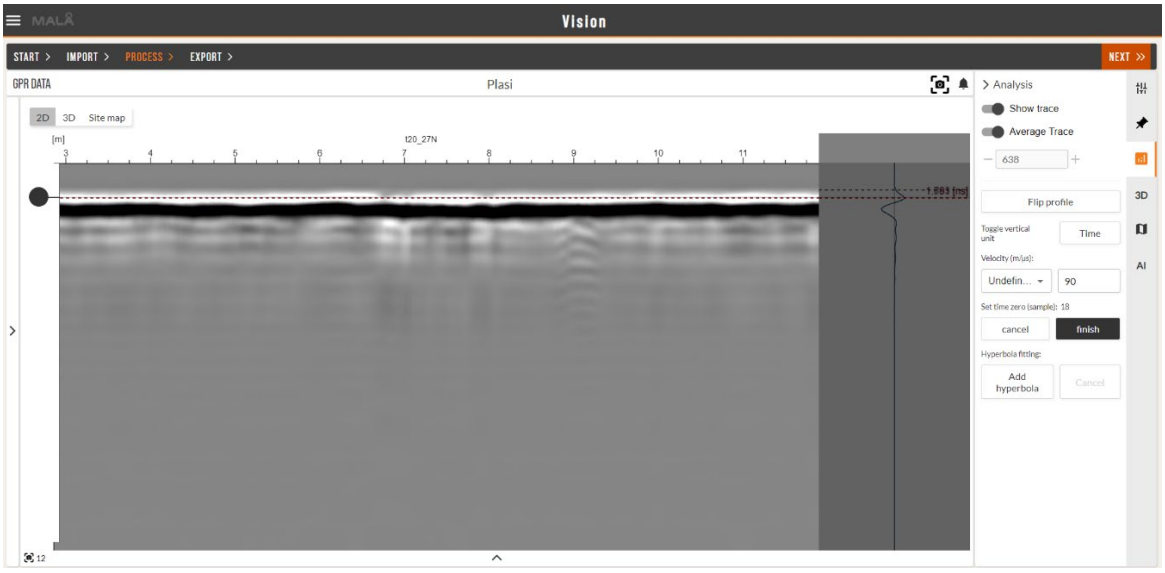

Figure 3.5: *Image depicting the application of Time-zero correction. (MALÅ Vision software)*

The next step to be taken was to perform the velocity analysis and conversion of travel time to depth. For the velocity analysis MALÅ Vision offers the Hyperbola fitting method, but due to the data not having any hyperbola clear enough to perform this method, the velocity was chosen from literature, concerning the lithology of the survey area, and set manually to 90 $m/\mu s$. Once the proper velocity

was chosen, the conversion of travel time to depth could be done automatically by pressing the ‘’**time**’’ button next to the ‘’***Toggle vertical unit***’’ option (fig. 3.6).

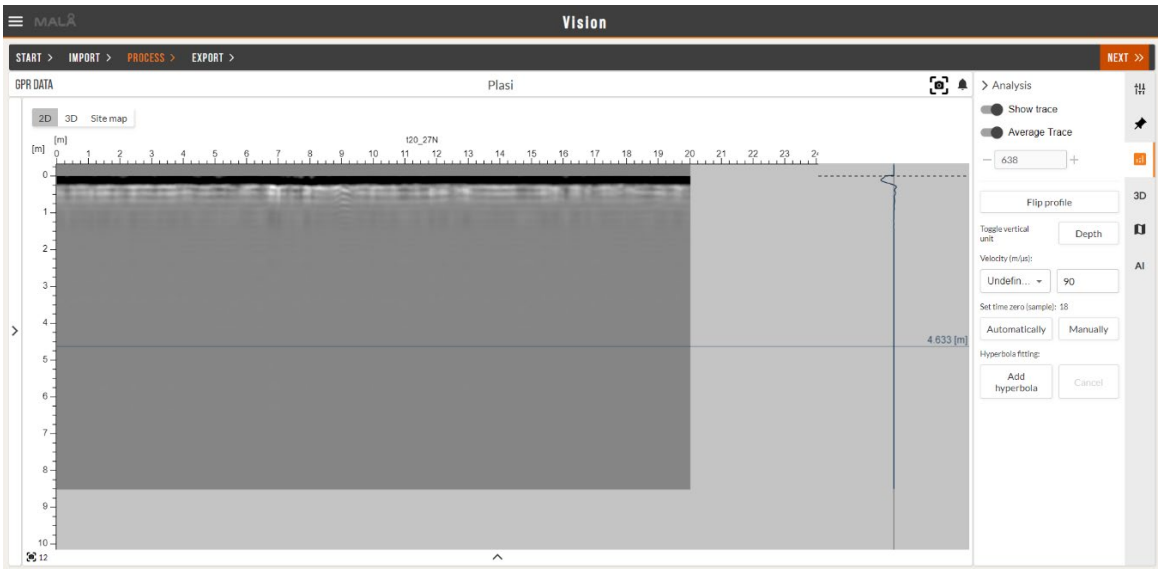

Figure 3.6: *Image depicting the conversion of travel time to depth (MALÅ Vision software)*

In order to make the data clearer and reduce the noise generated from random sources, the **background removal** option was chosen from the filters section with ‘’***Window length*** ‘’ set to 300 (fig. 3.7).

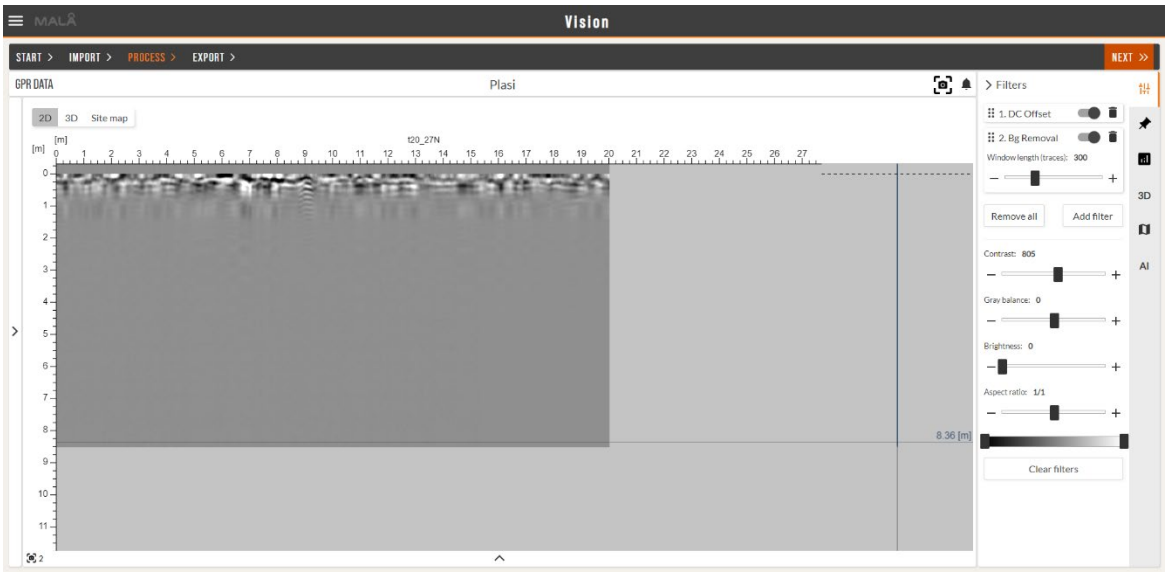

Figure 3.7: *Image depicting the application of the background removal filter with ‘’Window length ‘’ set to 300ns (MALÅ Vision software).*

After the background noise was removed, a gain filter was applied to the profiles to make the remnant reflections of interest more prominent. MALÅ Vision gives us 3 options to apply the gain filter. Taking into consideration the characteristics of the data and the goal of the investigation, the ***Linear gain*** option was chosen with a **slope** set at 10 (fig. 3.8).

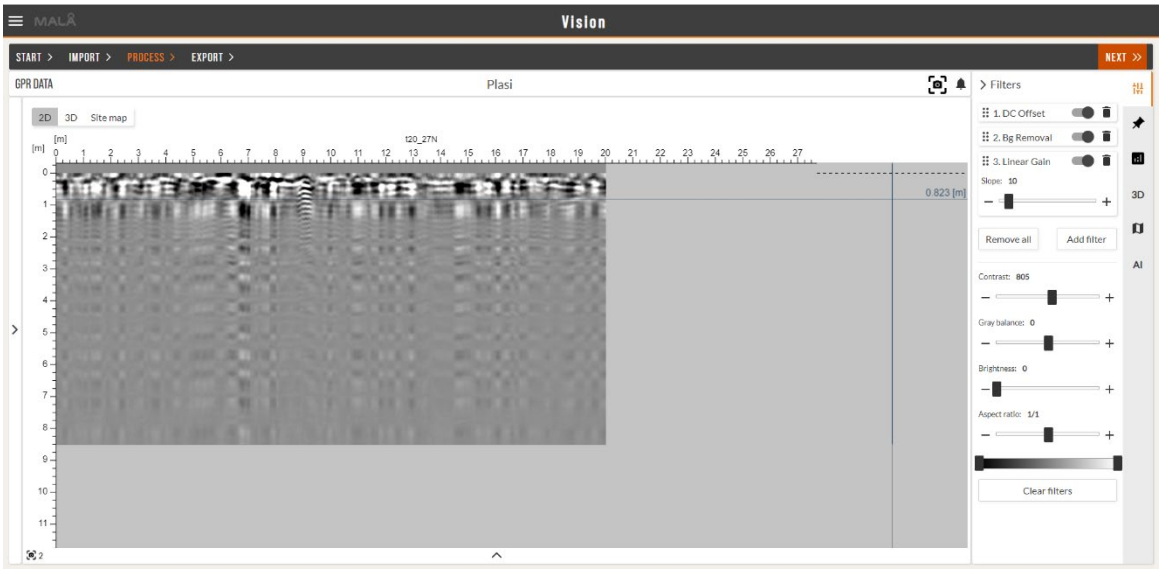

Figure 3.8: *Image depicting the application of the Linear gain filter. (MALÅ Vision software)*

The next processing method applied was a **Bandpass filter** in order to increase the *Signal to Noise* Ratio (SNR). This is achieved by filtering out signal components with frequencies that are outside the main working bandwidth of the GPR system. In this study the GPR working frequency was 250 MHz, by following a common practical rule which states that the lower threshold of a bandpass filter should be **half** the GPR antenna frequency and the upper threshold should be **double** the GPR antenna frequency, the bandpass filter was set approximately between 100 MHz – 400 MHz (fig. 3.9).

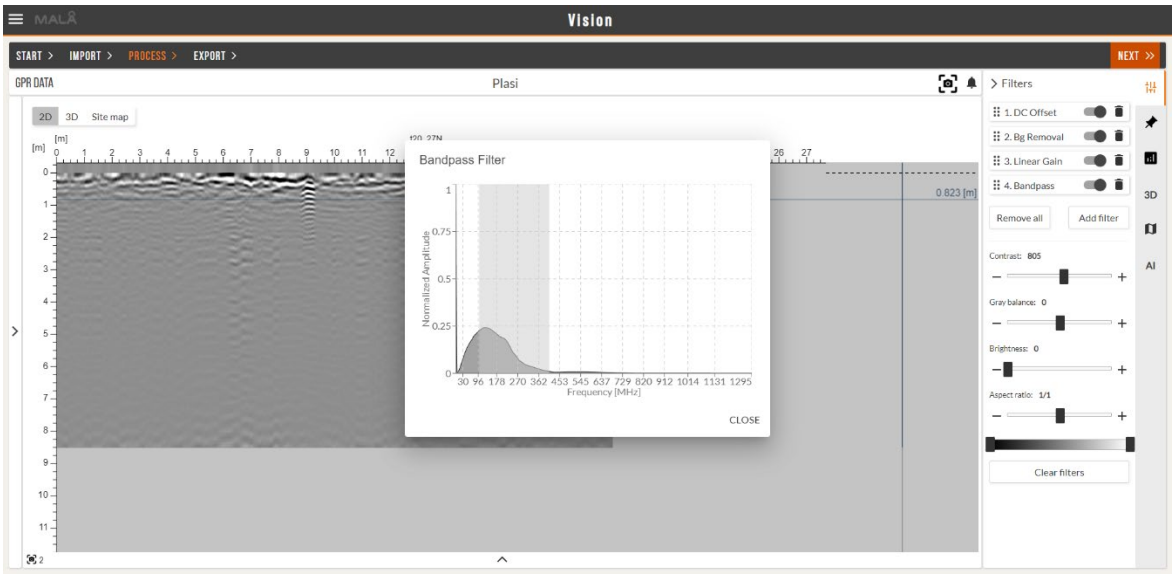

Figure 3.9: *Image depicting the application of the Bandpass filter with the frequency set at 100 MHz – 400 MHz (MALÅ Vision software).*

The last and one of the most important processing methods that was applied on the GPR data was the **Migration.** By applying the F-K migration filter that is provided by the software and setting the velocity to 90 $m/\mu s$**.** The result of this process is a profile less distorted by hyperbolas (fig. 3.10).

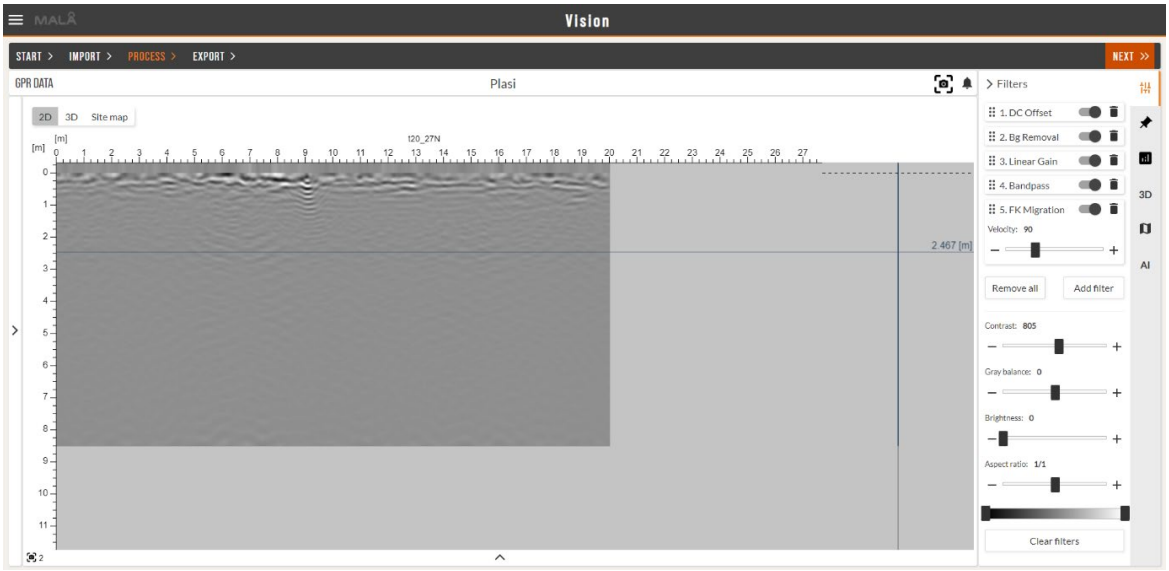

Figure 3.10: *Image depicting the application of the migration filter with the value set at 90 m/μs (MALÅ Vision software).*

4. Final results and interpretation

In MALÅ Vision 3D interpolation can be carried out using the following techniques:

- Inverse distance weighting
- Linear
- Bilinear
- FK Pocs 3D

Out of all these interpolation techniques that are provided, taking into consideration the data that was available, the Bilinear technique was applied. This interpolation technique is best suited for data collected in two directions as it performs a linear interpolation in both directions (X, Y) and averages the two results to yield a final result.

4.1 Final processing results

The results can be displayed as a **3D Cube**, through **Depth Slices** and as an **Iso Surface**. Below the final Depth Slices are presented after the data have been processed and interpolated using the MALÅ Vision software. Each Depth slice displays the results of the interpolation at a certain depth. From a geophysical perspective, the following information can be derived:

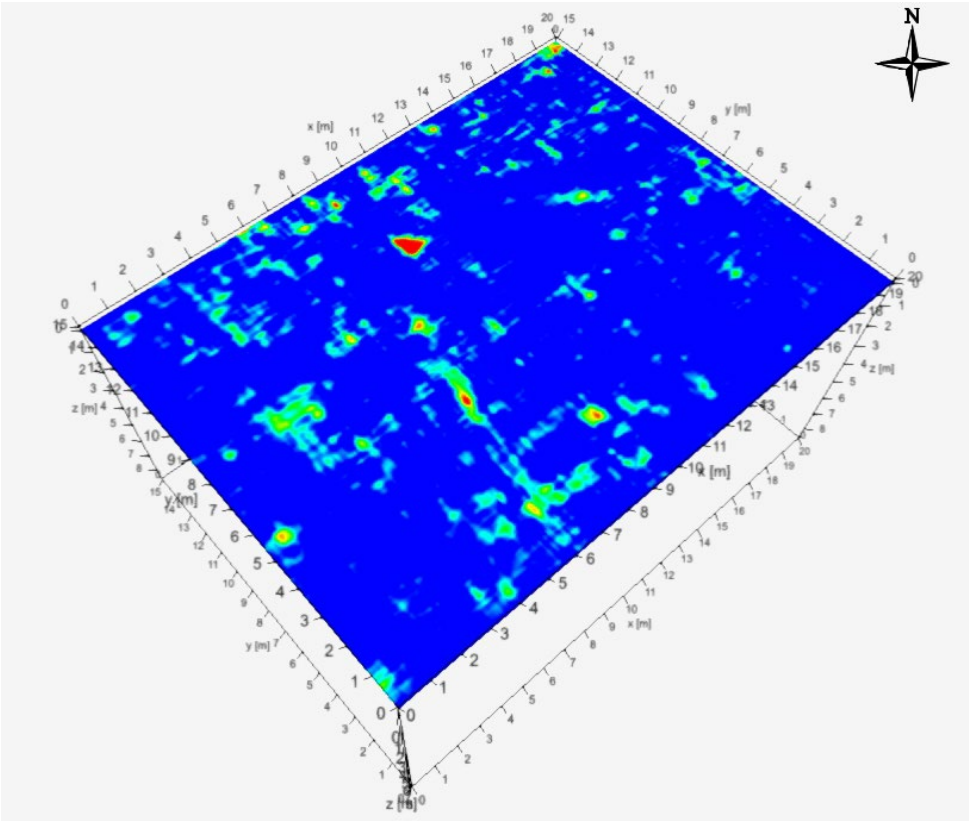

Figure 4.1: *Final results (depth slice) at 20cm depth.*

Depth slice 2 (fig. 4.1) displays the processed data from a depth of 20 cm. It is the first Depth slice that gives us information about a few areas with strong reflections and is indicative of additional areas that might be of interest at greater depths. The positions where the most signal reflections can be observed are the following:

- At X(9-10m), Y(11-12m) there is a relatively small area with very strong reflections.
- At X(6-7m), Y(1-9m) there is an area with linear geometry and direction spreading from WNW to ESE. This area has both stronger and weaker signal reflections.
- At X(6-11m), Y(14-15m) there are various targets created from stronger and weaker signal reflections.

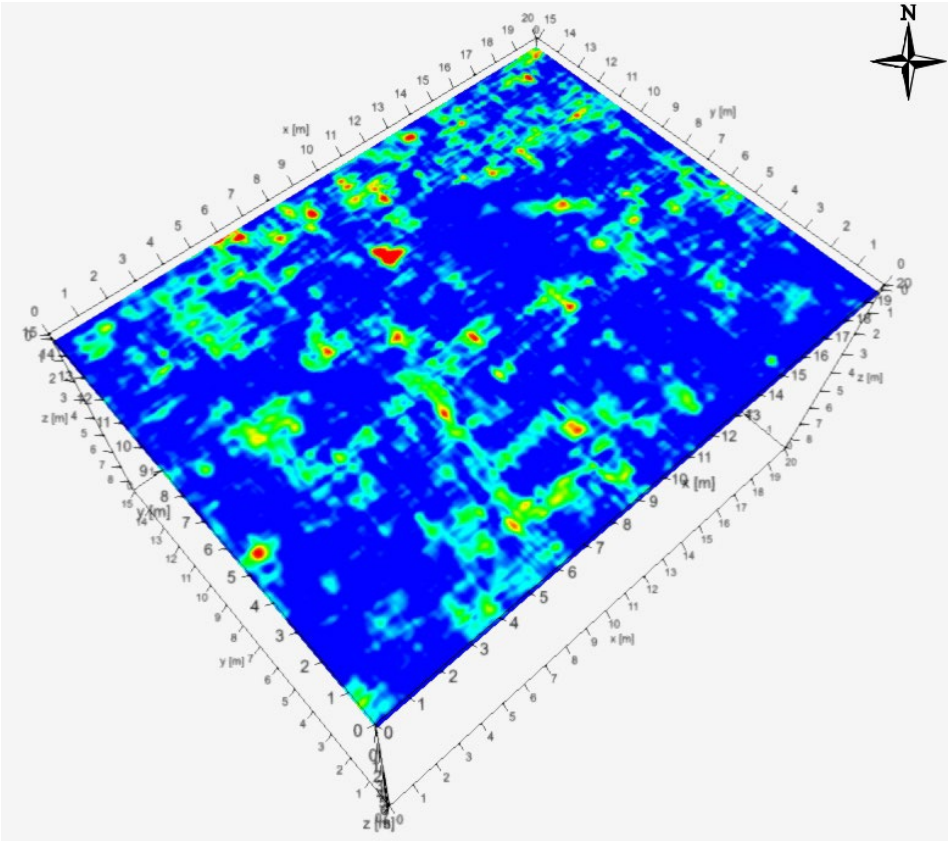

Figure 4.2: *Final results (depth slice) at 40cm depth.*

Depth slice 4 (fig. 4.2) displays the processed data from a depth of 40 cm. The areas with strong signal reflections that were present in depth slice 2 can be seen at this depth as well, and the areas with weaker signal reflections have become even more prominent. The positions of the areas where the most signal reflections occur are the following:

- At X(1-20m), Y(10-15m) there is an area with a plethora of targets caused by both stronger and weaker signal reflections. This area spreads in a linear manner with a direction NNE-SSW
- At the center of the investigation area there are multiple targets that are spread at different directions some being parallel and some perpendicular to each other. A few examples are X(4-10m), Y(1-3m) and X(6-9m), Y(5-9m).

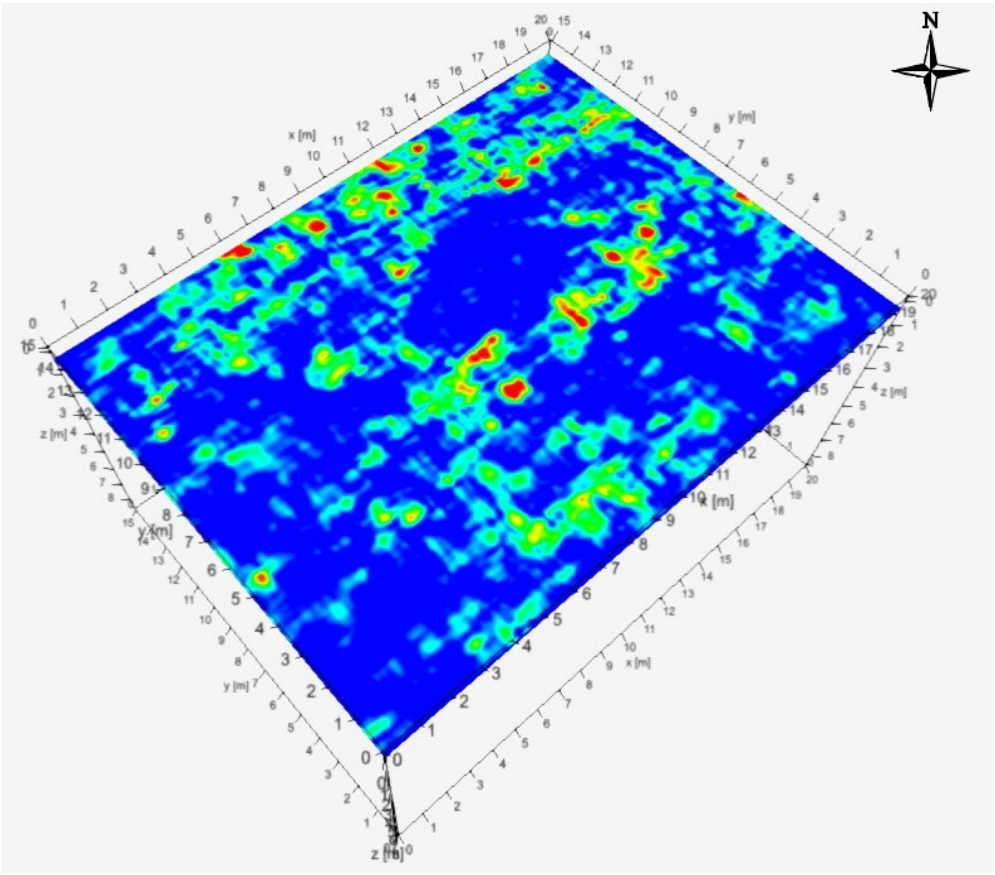

Figure 4.3: *Final results (depth slice) at 60cm depth.*

Depth slice 6 (fig. 4.3) displays the processed data from a depth of 60 cm and it is the one where the most signal reflections can be observed.

The positions of the areas where the most signal reflections occur are the following:

- At X(3-18m), Y(11-15m) and X(7-17m), Y(6-8m) multiple targets can be observed which are spread in a linear manner in a direction of NNE-SSW.
- Another noticeable area with multiple targets but with a weaker signal reflection intensity than the previous ones is located at X(6-12m), Y(1-2m). These targets have the same direction as before at NNE-SSW.

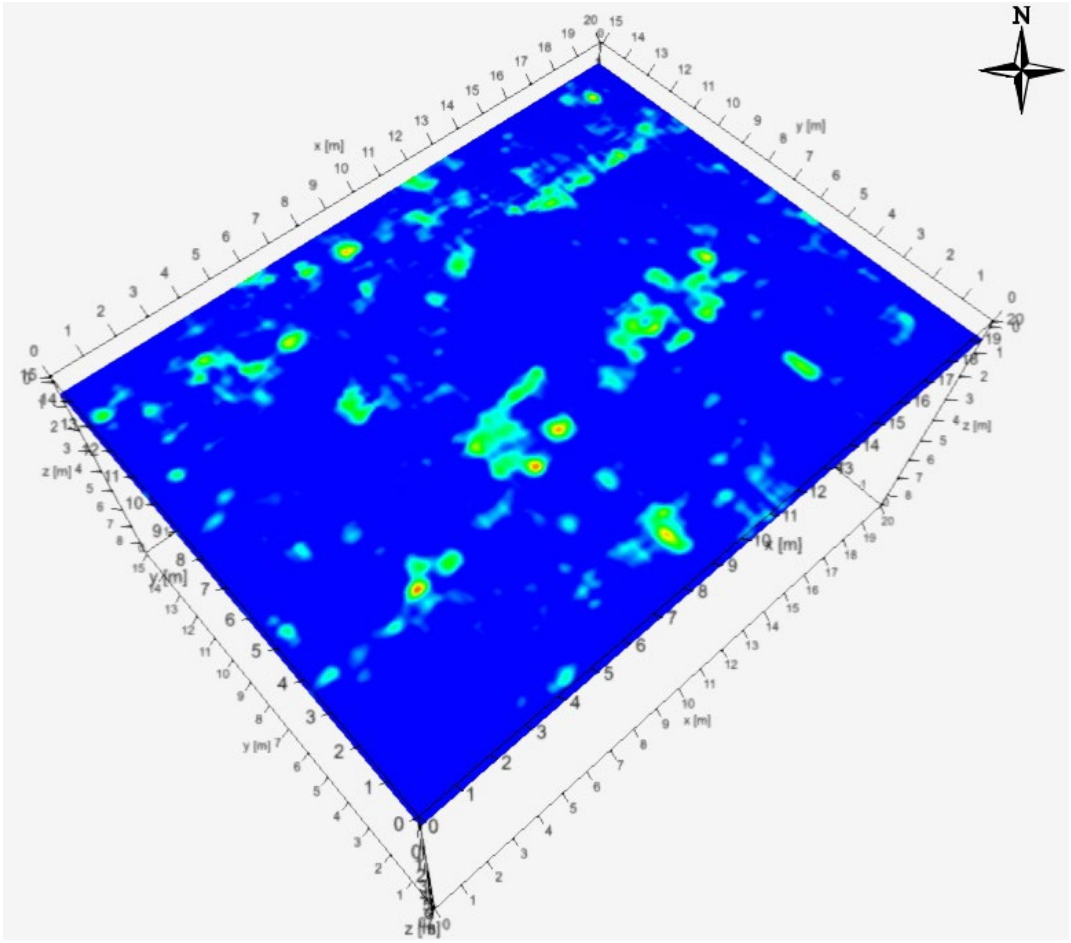

Figure 4.4: *Final results (depth slice) at 80cm depth.*

Depth slice 8 (fig. 4.4) displays the processed data from a depth of 80 cm. On controversy to the previous depth slices (figs 4.2 and 4.3), on this one the signal reflections start to reduce in strength. The few positions where signal reflections are noticeable are at X(4-6m), Y(3-16m) . There are a few areas with some noticeable targets, such as X (4-6m), Y(7,10m) and X (4-6m), Y(12,15m) but they do not seem to have a continuous linear spread because there are no signal reflections being detected from positions in between those areas.

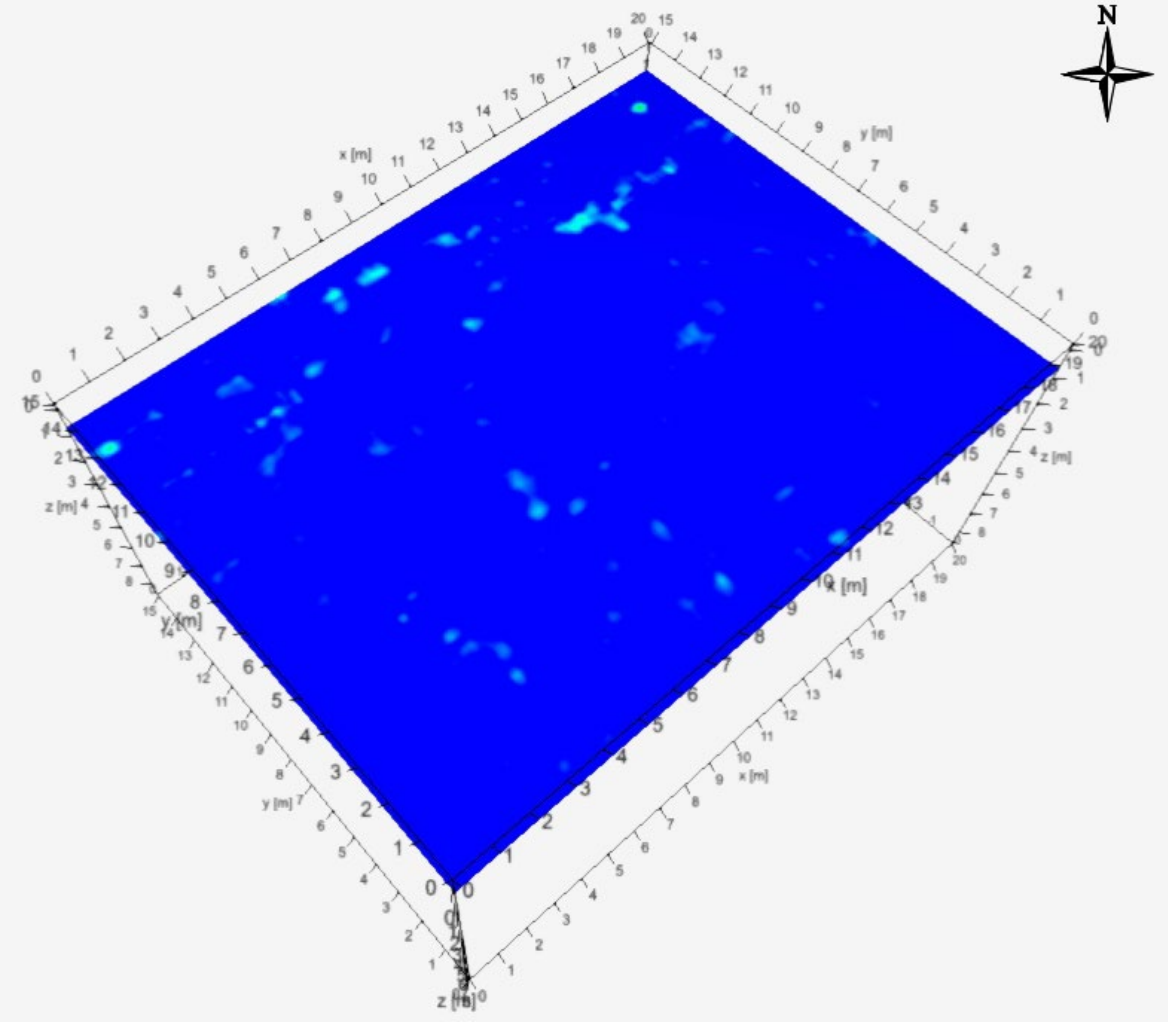

Figure 4.5: *Final results (depth slice) at 1m depth.*

Depth slice 10 (fig. 4.5) displays the processed data from a depth of 1 m and is the last Depth slice where any signal reflections are still visible, but no target areas of importance can be determined. From depths higher than 1 m there are no reflections detected at all.

4.2 Interpretation

As it is mentioned before (§1) the region that the geophysical investigations took place is connected to the ancient city of Marathon. Previous investigations that have been conducted in the area have yielded great results in discovering remnants of the city, but the majority of its infrastructures have not been fully discovered yet. Using all the available geophysical and archeological information, the main goal of this investigation was to identify structures that resembled the geometry of architectonical remains. Having that in mind and taking into consideration the characteristics of the equipment as well as the methodology parameters chosen for the data acquisition, the following areas of potential archaeological interest were identified from each depth slice:

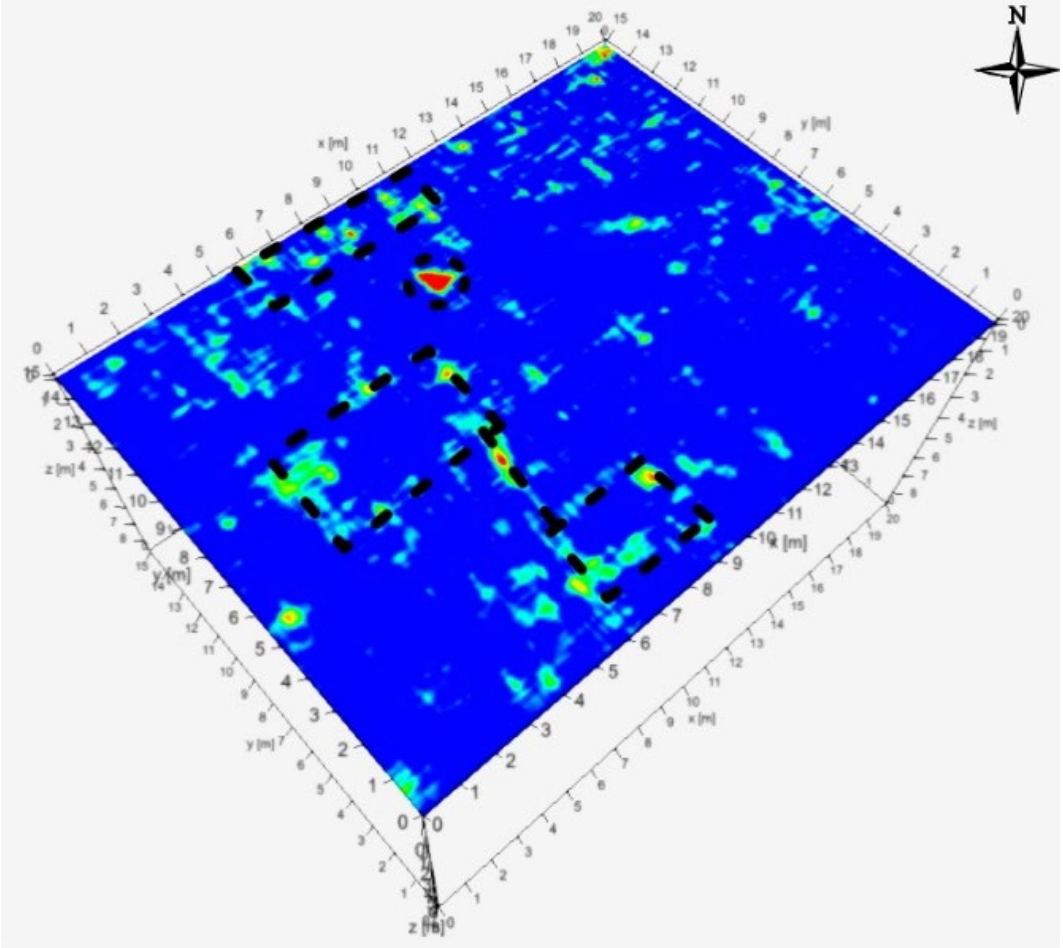

Figure 4.6: *GPR depth slice at 20cm, displaying potential areas of interest (black dotted lines).*

From Depth slice 2 at a depth of 20 cm, 2 target areas can be observed with rectangular geometry connected with a linear smaller area. This type of geometry could indicate the existence of two buildings remains from the ancient city. Furthermore, at the west part of the investigated area there are multiple targets spread in a linear manner which could be indicative of a wall.

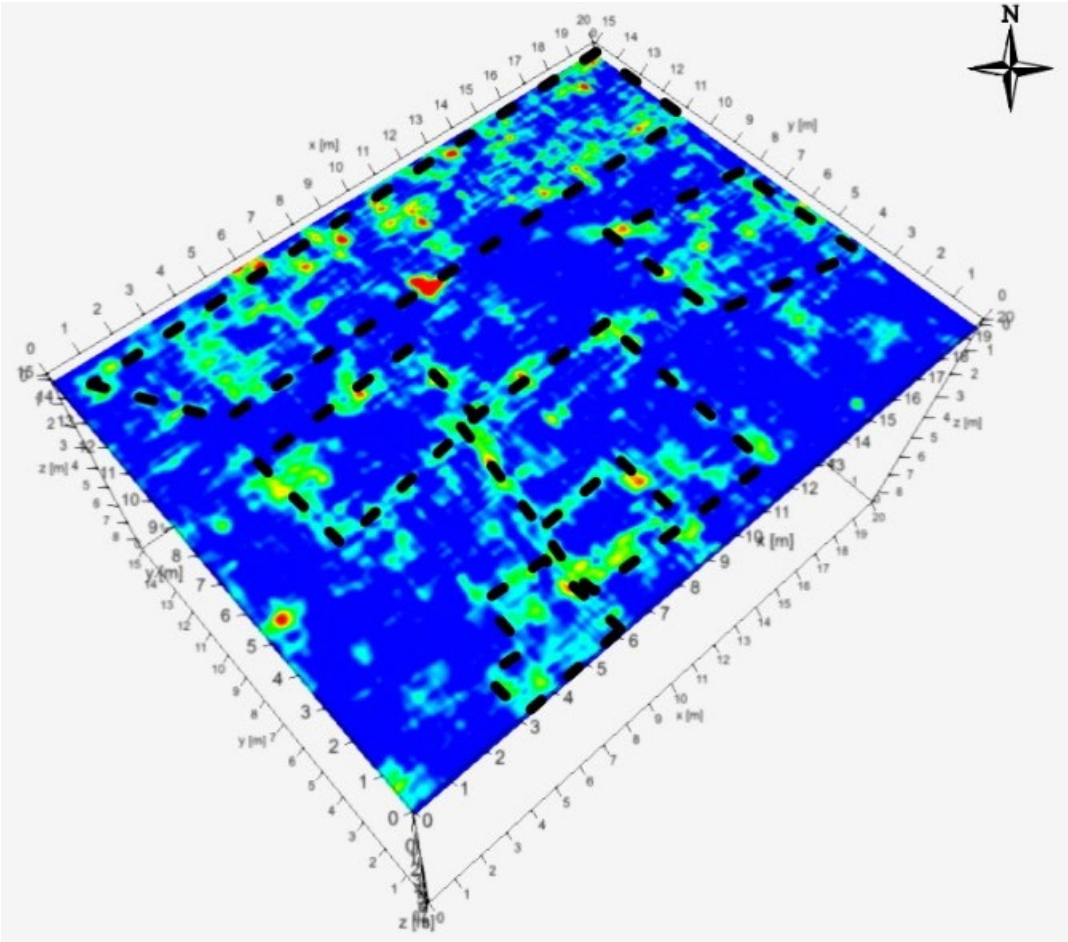

Figure 4.7: *GPR depth slice at 40cm, displaying potential areas of interest (black dotted lines).*

In figure 4.7, the geometrical characteristics of the previous areas of interest that are depicted in figure 4.6, seem to be even more defined. At this depth (40 cm) there are multiple areas of potential archeological interest, with the bigger one being in the west part of the study area. It is a large area with a plethora of targets placed in a linear manner that could be associated with the existence of a large outside wall, perhaps for the ancient city's protection. At the center and to the east, there are various target areas with rectangular geometry, indicating the existence of potential building foundations.

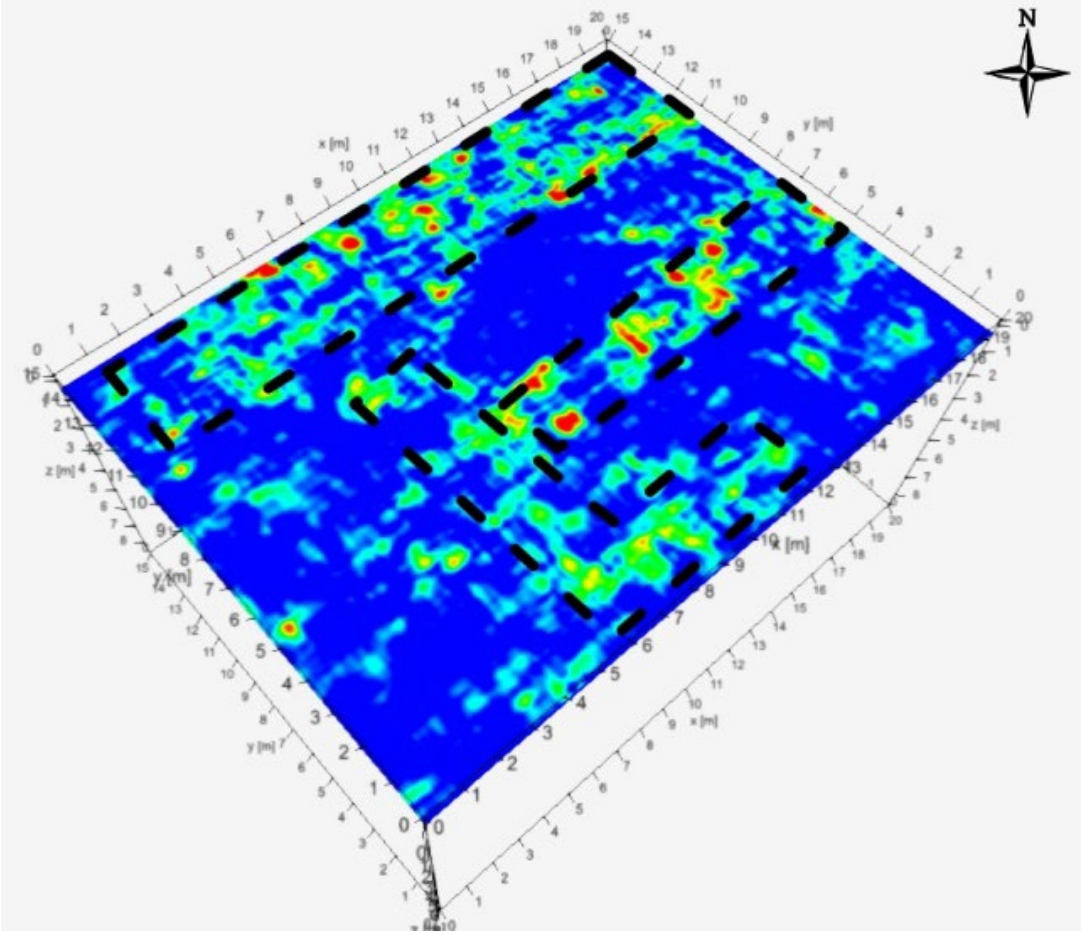

Figure 4.8: *GPR depth slice at 60cm, displaying potential areas of interest (black dotted lines).*

In figure 4.8 at a depth of 60 cm, the large linear area at the west part of the investigation is still visible and has become even more prominent reinforcing the idea that it might be part of the outside wall of the ancient city. Another area of interest that is displayed with the same geometry and parallel to the previous area is located at the center of the investigation and spreading NE. Due to the fact that it shows similarities with the previous area it can also be considered as a potential wall of a bigger infrastructure. The final area of interest that has been identified, is located at the center of the investigation area spreading ESE and having a different geometry in comparison to the previous Depth slices. This identified area could also be part of a broader infrastructure.

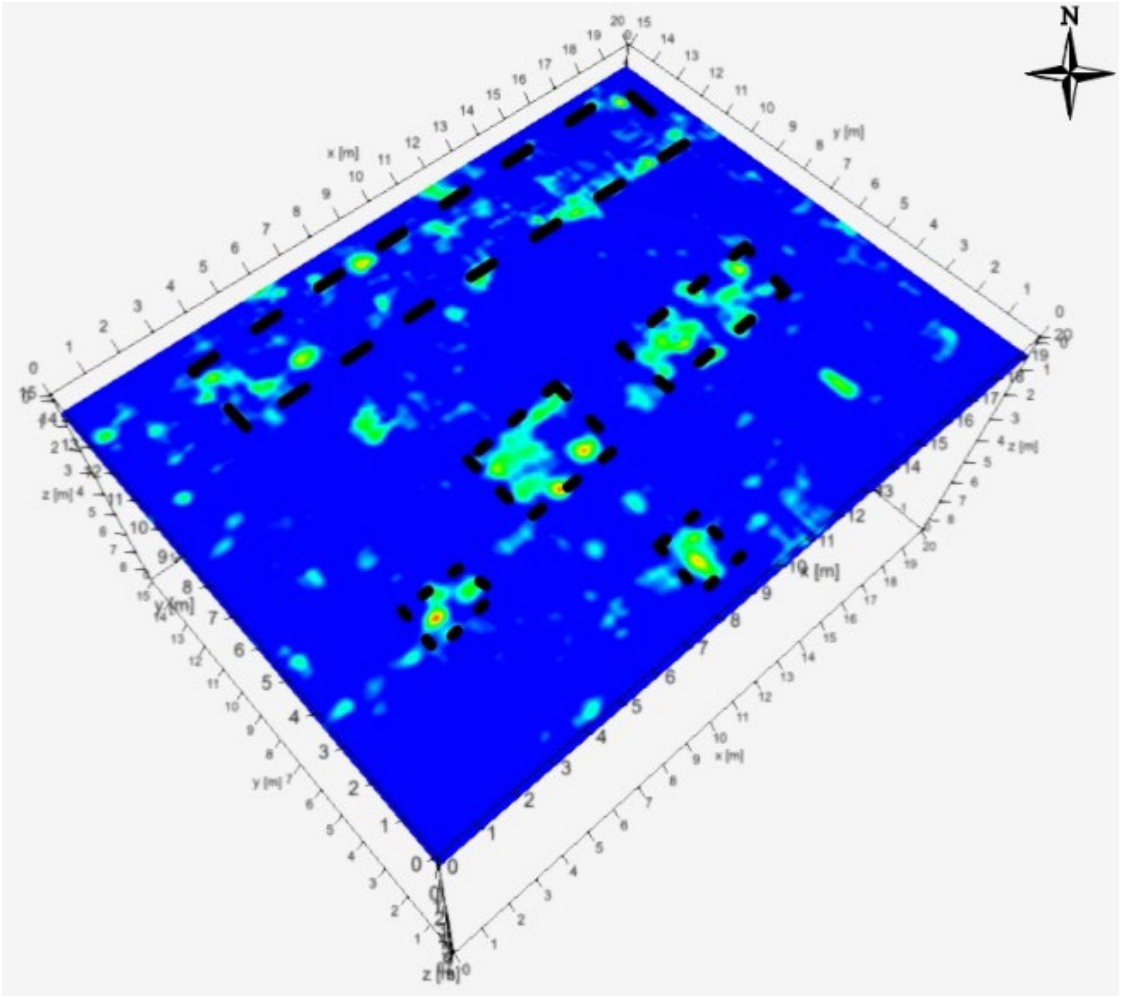

Figure 4.9: *GPR depth slice at 80cm, displaying potential areas of interest (black dotted lines).*

In figure 4.9, at the depth of 80 cm, the intensity of the signal reflections has been drastically reduced in comparison to the previous Depth slices (fig 4.7 and 4.8). At this depth, there is not enough information to identify new areas of archaeological interest, but at least we can see the spatial distribution of the remnants of the previous linear targets.

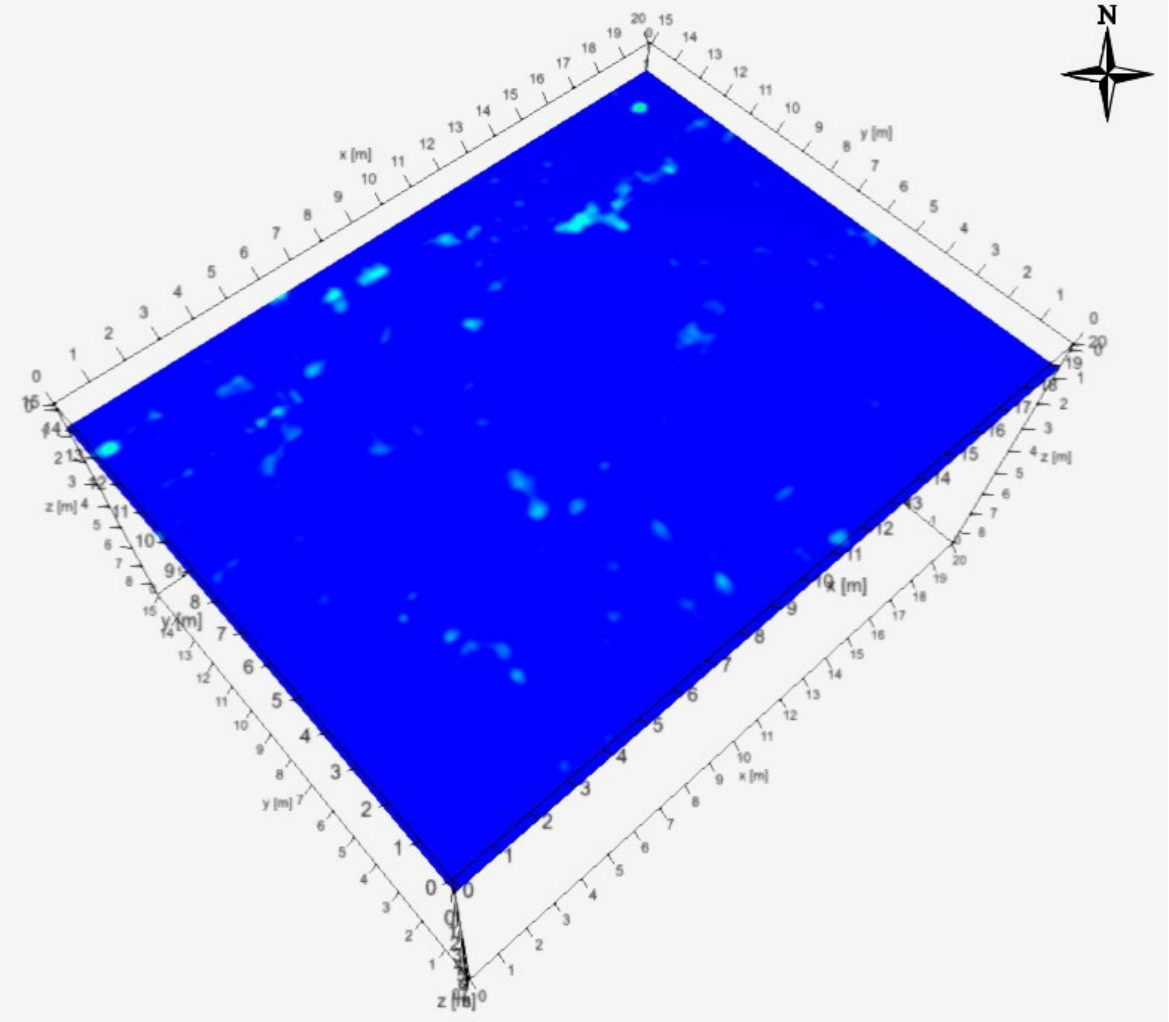

Figure 4.10: *GPR depth slice at 1m depth , displaying* ***NO*** *geophysical targets/potential areas of interest.*

From figure 4.10 it can be clearly seen that there is no more information about any targets at all. This might be because of the attenuation of the GPR signal due to the soil being conductive, thus prohibiting the GPR to acquire data from deeper targets. Another fact could also be that there might not be any archaeological targets past 1m of depth.

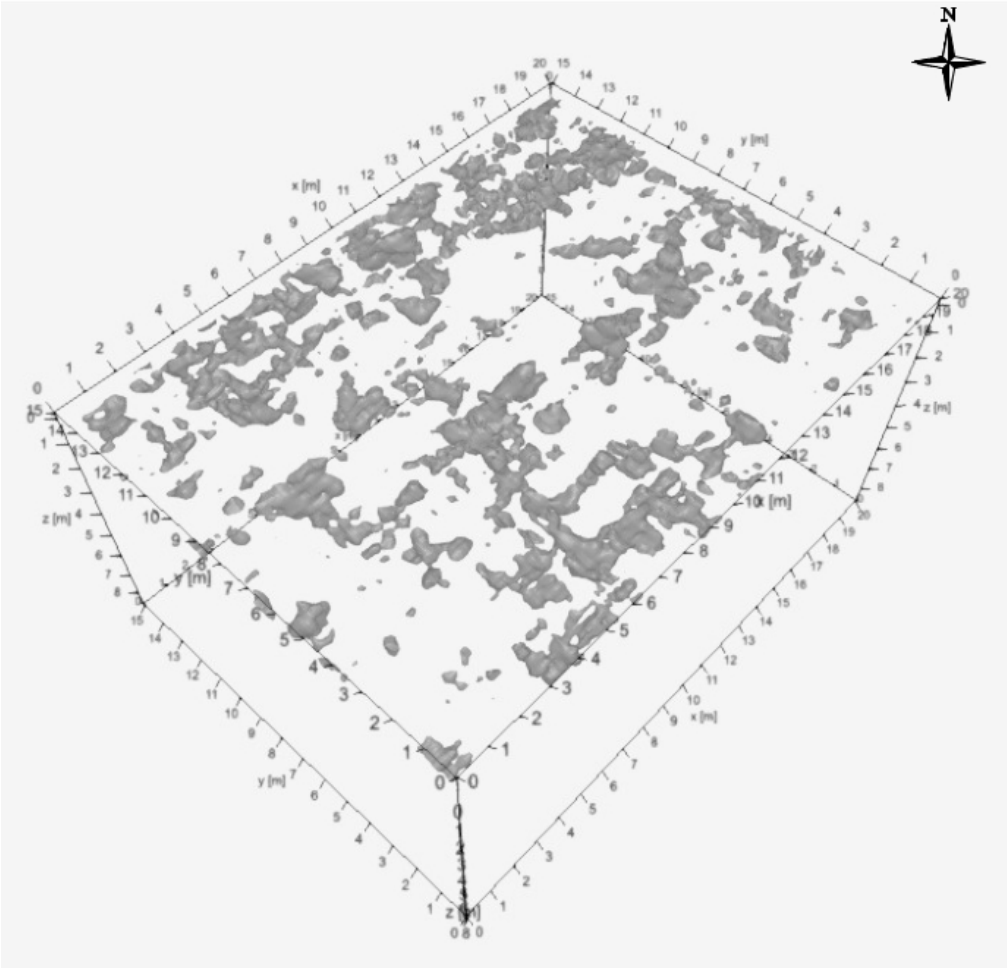

Figure 4.11: *Final result displaying the volume of the reflected signals throughout the area being investigated.*

Finally, the results are also displayed as iso surfaces. Using this method, we can observe the spatial distribution of the reflected GPR signals in 3D presentation. The volume of data that is depicted is proportionate to the intensity of the signals being reflected, with higher reflection intensity generating greater volumes. The results of this display method have a great similarity with the results depicted in the 2D depth slices showing the same areas of interest as described above, with the majority of the volumes concentrated between 40 – 60 cm of depth (fig. 4.11).

4.3 Conclusions - Discussion

The archaeological excavations that took place in the area prior to the geophysical survey, revealed multiple architectural/archeological remains with a geometrical spatial distribution at shallow depths between 20-80 cm. The archaeological information that was provided, gave us a clear indication on the proper investigation depth and the possible geometrical characteristics of the geophysical targets. The geometrical patterns throughout the geophysical survey could be associated with archaeological remains. For obvious reasons, archaeological investigations require a high resolution investigation, in order to yield the best results possible. Therefore, a dense grid was set in the area that the survey took place where 72 GPR profiles were caried out at different directions with a spacing of 0.5m. To improve the data even further, topographic measurements were taken for each profile, in order to create a high-resolution topographic background.

After analysing and processing the GPR data accordingly, by the results shown above (§4.1), the following conclusions can be made:

- In the first 20 cm of depth there are almost no GPR signals being reflected, and therefore no significant areas of archaeological interest.
- The strong reflections occur at depths between 20 - 60 cm, where areas of archaeological interest can be identified and marked. They have a prominent geometry that is indicative of archaeological/architectonical remains.
- From depths of 80 cm the signal intensity starts reducing and when we reach depths of 1m and above, there is no further information depicted.

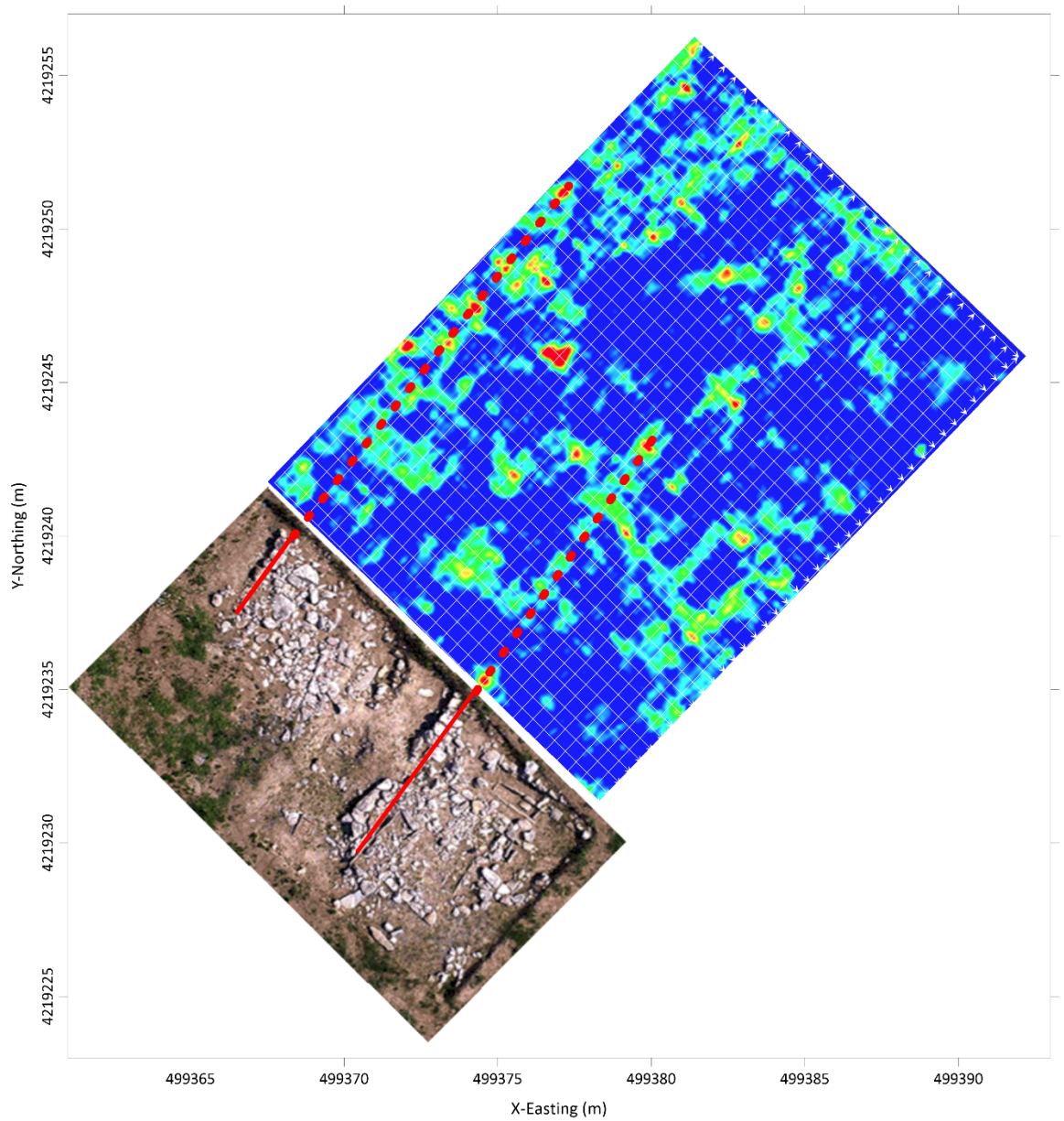

Figure 4.11: *GPR depth slice at 40cm, where the linear ancient remains in the archaeological trench seem to expand to the northeast (red dotted lines), as indicated from the GPR results.*

As it is mentioned before, previous research that has been carried out in the broader area of this survey, which has revealed archaeological remains between the depths of 20 – 80 cm. Taking this into consideration, the final results of this detailed geophysical investigation are in accordance with the previous studies and with the archaeological excavations, making the assumptions about the possible areas of archaeological interest even more plausible. More specifically, the GPR results (depth slice at 40cm) highlighted linear structures, which seem to be an extension of the ancient remains revealed by the archaeological excavations (fig. 4.11).

Last but not least, the fact that there is no further information at depths greater than 1m could be attributed to either the high levels of signal attenuation that occur due to the soil being very conductive, because of the survey area proximity to the sea, or simply because there are no more archaeological remains in greater depths, with the first assumption to be more possible.

.

Bibliography

https://gpg.geosci.xyz/content/GPR/index.html

Andrea Benedetto, Fabio TostiLuca, Bianchini Ciampoli, Fabrizio D'Amico (2016): An overview of ground-penetrating radar signal processing techniques for road inspections.

Annan, A.P. (2005). Ground penetrating radar, in near surface geophysics, in D.K. Butler (eds), Society of Exploration Geophysicists, Tulsa, OK, USA, Investigations in Geophysics No. 13, pp. 357–438.

Annan, A.P. (2009). Chapter 1 - Electromagnetic Principles of Ground Penetrating Radar. In Ground Penetrating Radar Theory and Applications, Harry M. Jol, ed. (Amsterdam: Elsevier), pp. 1–40.

Cassidy, N.J. (2009). Chapter 2 - Electrical and Magnetic Properties of Rocks, Soils and Fluids. In Ground Penetrating Radar Theory and Applications, Harry M. Jol, ed. (Amsterdam: Elsevier), pp. 41–72.

Conyers, Lawrence B. (2009). Ground-penetrating radar for landscape archaeology. In: Campana, Stefano & Salvatore Piro (eds.) Seeing the Unseen-Geophysics and Landscape Archaeology, pp. 245–56. CRC Press/Balkema: Taylor and Francis Group, London.

David J. Daniels (2004). Ground Penetrating Radar (2nd Edition)

Erica Carrick Utsi (2017). Ground Penetrating Radar, Theory and Practice

Everett, M. E. (2013). Near-Surface Applied Geophysics, Cambridge University Press.

Jol, M., Harry (2009). Ground penetrating radar: Theory and Applications, Elsevier Science

Lozios, S. (1993). Tectonic Analysis of Transformed Formations of Northeast Attica. PhD thesis, 317 pp., Athens 1993. (in Greek)

MALÅ-Vision-User-Manual-May-2022-1

Polychronakou-Sgouritsa, Naya, Papadatos, Yiannis, Balitsari, Anthi and Prevedorou, Eleanna. (2016). Marathon in the Middle and Late Bronze Age: New Evidence from an Old Excavation. Preliminary Results from the Excavation of the 83 University of Athens at Plasi. J. Driessen (ed.) Ra-pi-ne-u: Studies on the Mycenaean World offered to Robert Laffineur for his 70th Birthday, Aegis 10, Louvain-la-Neuve: Presses universitaires de Louvain. p. 305-315.